Fusion Engineering and Design 221 (2025) 115394

Contents lists available at ScienceDirect

Fusion Engineering and Design

journal homepage: www.elsevier.com/locate/fusengdes

Low cycle fatigue life prediction for neutron-irradiated and nonirradiated RAFM steels via machine learning

Hussein Zahran [a,b,c], Aleksandr Zinovev [a], Dmitry Terentyev [a], Ali Aouf [d,e], Magd Abdel Wahab [b,f,g,*]

[a] Structural Materials Group, Institute for Nuclear Energy Technology, Belgian Nuclear Research Centre SCK CEN, Mol 2400, Belgium
[b] Soete Laboratory, Department of Electrical Energy, Metals, Mechanical Constructions and Systems, Faculty of Engineering and Architecture, Ghent University, Ghent 9000, Belgium
[c] Department of Design and Production Engineering, Faculty of Engineering, Ain Shams University, Cairo, Egypt
[d] Engineered and Geosystems Analysis Group, Institute of Sustainable Waste and Decommissioning, Belgian Nuclear Research Centre SCK CEN, Mol 2400, Belgium
[e] Université Catholique de Louvain, Louvain-la-Neuve 1348, Belgium
[f] College of Engineering, Yuan Ze University, Taiwan
[g] Parallel and Distributed Systems Laboratory, Jožef Stefan Institute, Jamova cesta 39, Ljubljana SI-1000, Slovenija

ARTICLE INFO

Keywords:
EUROFER97
Low cycle fatigue
Reduced Activation Ferritic-Martensitic
Machine Learning

ABSTRACT

EUROFER97 and other Reduced Activation Ferritic-Martensitic (RAFM) steels are candidate structural materials for fusion reactors. Qualification of these steels requires the assessment of their performance under fatigue loading especially after exposure to neutron irradiation. However, the significantly high costs and engineering complexity of performing such tests make the experiments on irradiated material difficult. Therefore, alternative methods to predict the fatigue life of RAFM steels are deemed beneficial. In this study, machine learning was used to predict the fatigue life of irradiated and non-irradiated RAFM steels utilizing published experimental data. Four algorithms were benchmarked: Random Forest Regression (RF), Support Vector Regressor (SVR), Gradient Boosted Regressor (GBR), and MultiLayer Perceptron (MLP). Predictions were made based on two scenarios: one scenario with yield strength as input along with the fatigue test condition, and the second scenario without the yield strength. The results showed that RF and GBR were the best performing algorithms, with R^2 score between 0.9522 and 0.9696 on the training set and between 0.9058 and 0.9249 on the validation set. The Mean Absolute Percentage Error (MAPE) score was between 0.3 and 0.43 % on the training set and 0.7 and 1.2 % on the validation set. The quality of prediction of fatigue life without using the yield strength was shown to be almost equal to that in the first scenario. SHAP analysis revealed that strain range was the most influential input feature, while GBR showed greater sensitivity to secondary features such as temperature and diameter. GBR also captured more nuanced interactions between input variables, particularly in irradiated datasets, confirming its superior ability to model complex fatigue behaviour. The ability of these algorithms to predict the fatigue life corresponding to test conditions not used for training was checked using 15 % of the collected database as a prediction set, which included fatigue life of irradiated materials. Results indicated that these algorithms were able to predict the fatigue life of this set with 83-87 % of the points lying within the factor of two from the experimental value.

Introduction

Thermomechanical fatigue is considered to be one of the main factors defining the lifetime of structural components in fusion reactors [1]. The European fusion roadmap includes major milestones for the future: ITER and DEMO. These tokamak-type fusion reactors have a cyclic work-mode. Besides that, plasma instabilities such as Multifaceted Asymmetric Radiation From the Edges (MARFEs) are expected to accompany plasma discharges [2,3]. Structural materials in the In-Vessel Components (IVC's) will have to withstand these operating conditions under 14 MeV neutron irradiation in a vacuum environment.

Qualification of EUROFER97 and other Reduced Activation Ferritic-

* Corresponding author.
E-mail address: magd.abdelwahab@UGent.be (M. Abdel Wahab).

https://doi.org/10.1016/j.fusengdes.2025.115394
Received 27 May 2025; Received in revised form 5 August 2025; Accepted 8 August 2025
Available online 14 August 2025
0920-3796/

Martensitic (RAFM) steels [4–9] requires extensive Low Cycle Fatigue (LCF) experimental campaigns under different testing conditions (temperatures, media) and under relevant neutron irradiation doses. Several experimental campaigns [10–14] were performed to assess the ageing of RAFM steels under low and high dose neutron irradiation corresponding to the expected doses in the ITER test blanket module (3 dpa), and the DEMO breeder blanket (20-50 dpa). The aim of these studies was to aid the development of specific design codes, for example the DEMO Design Criteria for In-Vessel Components (DDC-IC) by the EUROfusion Consortium [15,16]. However, the availability of LCF results for neutron irradiated specimens is limited due to the complexity and high cost of performing such tests. Therefore, methods to predict fatigue life are deemed beneficial [17].

The fatigue performance of RAFM steels under cyclic loading is governed by test medium, specimen geometry, and irradiation effects [18]. These factors interact in complex ways to influence crack initiation, propagation, and fatigue life. Experiments showed that fatigue life is reduced when specimens are tested in air compared to vacuum. This degradation was attributed to oxidation-driven mechanisms that accelerate both crack initiation and propagation [19,20]. Specimen diameter also affects fatigue life. Specimens with a diameter of 1 mm demonstrated significantly shorter fatigue lives that those with a 7 mm diameter. This disparity is due to the increased proportion of oxidized volume in the smaller specimens [21].

Irradiation introduces more complexity to fatigue behaviour. At lower strain amplitudes, irradiated RAFM steels tend to show higher fatigue life compared to the unirradiated steels, which is attributed to irradiation-induced hardening. However, at higher strain ranges, the effect of irradiation becomes inconsistent. Some studies report a reduction in fatigue life after irradiation, while others observe an improvement [22].

In the current age of big data and high computation powers, machine learning (ML) uses computers to build models, predict, and quantify the uncertainties related to these predictions. ML algorithms are able to efficiently build correlations between data inputs and the desired output (s) [23–25]. Another advantage is their higher computational accuracy and efficiency for non-linear regression compared to conventional statistical methods [26–28].

The aim of this study is to predict the fatigue life of irradiated and non-irradiated RAFM steels. The performance of widely used ML algorithms from literature was assessed to select the best algorithm for prediction. Random Forest (RF), Support Vector Regression (SVR), MultiLayer Perceptron (MLP) as an ANN algorithm, and Gradient Boosting Regression (GBR) as a boosting algorithm were used for this purpose. A brief literature study on the prediction of fatigue life in RAFM steels is presented in section 2. The gathered LCF database is shown in section 2.1. The different ML algorithms used in the benchmarking process are presented in section 2.2 using the framework in section 2.3. Feature selection results are shown in section 3.1. The method benchmarking results are shown in section 3.2. The quality of the prediction of unseen test conditions are shown in section 3.3.

Related works

Traditional fatigue life prediction methods can be broadly categorized into physics-based, and data-driven, approaches. Physics-based methods rely on empirical equations and simulation models to describe fatigue damage evolution. On the other hand, data-driven methods rely entirely on the data and tries to numerically model the relationship between the influencing factors and the target outcome. Among these methods are machine learning models that use the available data to extract important features from the input data to predict the required behaviour such as fatigue life.

Physics-based methods

This subsection lists the contributions by previous works for physics-based methods predicting the fatigue life of RAFM steels.

- Numerical simulations based on Chaboche viscoplasticity equations and continuum damage mechanics have been performed to predict the fatigue life of RAFM steels in the nonirradiated [29–31] and irradiated conditions [32]. However, these models are time consuming in terms of running and parametrization times. In addition, parametrizing these models requires the availability of several LCF results at each temperature. This is a challenge when it comes to testing irradiated specimens as explained in the introduction section.
- Another way to solve this problem was to estimate the parameters of the Manson, Coffin, and Basquin equation [33–35] from tensile properties. Some studies were able to use this method to predict the fatigue life of non-irradiated RAFM steels in air and vacuum [36–38]. A study by Zahran et al. predicted the fatigue life of irradiated and non-irradiated RAFM steels using the same methodology [18]. In this study, it was established that test medium (air or vacuum) and specimen size have an effect on fatigue life. Therefore, they have to be accounted for when making the predictions.

The main problem with these previously mentioned physics-based methods is that they are knowledge-based, which means they rely on physics-based models or experiences in assuming the parameters of the equations. The challenge is that the effect of irradiation on the fatigue behaviour of RAFM steels is not yet fully understood. Initially, it was observed that fatigue life increases after irradiation especially for smaller strain ranges. In the study by Petersen et al., the behaviour of EUROFER97 after neutron irradiation was described as ‘ambiguous’ [39]. In another review study by the same authors, a scatter of fatigue life of irradiated RAFM steels was observed around the non-irradiated ones indicating little influence of irradiation on fatigue life [22].

Data-driven methods

- Few works were found on the use of ML for prediction of mechanical properties of RAFM steels, such as yield strength, ultimate tensile strength, total elongation, and impact energy after irradiation [40–44]. No studies were found on the prediction of the fatigue life of RAFM steels.
- ML has recently been used to predict the fatigue behaviour of metallic alloys in several studies [45–52]. Hei et al. [47] applied the RF and ANN methods to different steels, while Sai et al. [48] relied on RF, SVR, and boosting algorithms for multiprincipal element alloys.

Although several studies were done to predict the fatigue life of metallic alloys in literature, no studies were found on the prediction of the fatigue life of RAFM steels. In addition, no studies were found in the literature predicting the fatigue life of irradiated metallic alloys in general.

The different methods predicting fatigue life of RAFM steels in literature are summarized in Table 1.

From this table, the gap in literature is obvious. Therefore, the

Table 1
Summary of related works in literature predicting the fatigue life of RAFM steels.

Approach	Method	Non-irradiated RAFM steels	Irradiated RAFM steels
Physics-based	Numerical simulations	[29–31]	[32]
	Manson, Coffin, and Basquin equation	[36–38]	[18]
Data-driven	ML	**None**	
		Scope of this study	

novelty of this study is that this is the first study to apply ML methods to predict the fatigue life of RAFM steels, particularly including data from irradiated materials.

LCF database and ML algorithms

LCF database

The strain-controlled LCF results of various RAFM steels were gathered from open literature. There are various steels to be qualified as candidates for structural components in fusion reactors. The gathered database included LCF results of EUROFER97 [53], JLF-1 [54], F82H, [55] ARAA [56], In-RAFM [57], and CLAM steels [5]. The gathered database and the sources are summarized in Table 2 and Table 3 for the non-irradiated and irradiated RAFM steels respectively.

As mentioned in the introduction, the fatigue life of RAFM steels is affected by the specimen diameter, test medium, and irradiation dose. This is in addition to the test temperature and strain range with their well-known effects on fatigue life. Therefore, these parameters were used as input to the ML algorithms.

The database includes a total of 458 fatigue tests with 408 tests for non-irradiated material and 50 tests for irradiated material. It covers also different specimen diameters (1 – 10 mm), test media (air and vacuum), and irradiation doses (2.5 – 71 dpa). The distribution of input parameters and the output variable (fatigue life) are shown in Fig. 1 and Fig. 2 respectively. It can be observed that the number of tests for non-irradiated material (irradiation dose equal to zero in Fig. 1(d)) is significantly higher than those for irradiated material due to the engineering difficulties discussed in the introduction section). It is worth mentioning that this is the same LCF results database gathered for a previous study by authors [18] to which the reader might refer for the detailed test conditions, and for a statistical analysis of the effect of specimen diameter and test medium on fatigue life for RAFM steels.

Previous studies predicting fatigue life using ML used only the fatigue test conditions as input for the models [28,79] which is the essence of ML. Also, some recent studies used material properties such as tensile properties or chemical composition as inputs as well [47,80–82]. This was claimed to help generalize the application of the ML models on different materials within the same class. In this study, both scenarios were tested.

In Scenario 1, yield strength was chosen as the material parameter representing the material tensile properties. The reason for this choice is the possibility to extrapolate the yield strength of the material at irradiation doses under which tensile tests are not yet available through the irradiation induced hardening curves [32]. In addition to this, the effect of thermo-mechanical heat treatment plays a more significant role in the resulting yield strength of RAFM steels compared to the chemical composition. The solid solution contribution to yield strength is minor compared to the dislocation forest hardening, dislocation-precipitate pinning, and the Hall-Petch effect due to laths. In this case, yield strength would represent the chemical composition and the thermo-mechanical heat treatment of the RAFM steels [83–87]. Yield strength would then be an input in addition to the fatigue test conditions: specimen diameter, irradiation/test temperature, test medium, irradiation dose, and applied strain range.

Since the difference in yield strength at a given temperature was found to be relatively small between the different RAFM steels, Scenario 2 was considered in the present work disregarding yield strength and using only the mentioned fatigue test conditions as inputs to the machine learning model.

The yield strength of the RAFM steels at the same test conditions of the gathered LCF database were gathered from literature as well and their values are listed in Table 4 and Table 5 for the non-irradiated and irradiated RAFM steels respectively.

ML algorithms

In this study, four different ML algorithms were benchmarked to assess their ability to predict the fatigue life of RAFM steels. The four algorithms are RF, SVR, MLP, and GBR. The input features and the output targets were extracted from the gathered LCF database as described in section 2.1. The following subsections outline the theoretical background of each algorithm with details on the method of handling the input features. The full implementation of these algorithms is then described in section 2.4.

RF

RF is an ensemble supervised ML algorithm that combines the ensemble learning and the non-linear statistical approaches [94,95], and it builds multiple decision trees (a hierarchical supervised-learning algorithm) to improve the overall accuracy and robustness. Each tree is trained on a random subset of the data using a bootstrap aggregation method [96] ensuring diverse model perspectives and reducing

Table 3
Test conditions and sources for the database of LCF tests of irradiated RAFM steel specimens as obtained from open literature.

Material	Test medium	Irradiation campaign	Irradiation dose (dpa)	Irradiation/test temperature (°C)
E97-1	Air	SOSIA-02	2.5	300 [58]
	Vacuum	HFR Phase-IIb (SPICE)	16.3	250 [63]
				350 [63]
				450 [63]
	Air	ARBOR 1	30.2	330 [59]
		ARBOR 2	71	330 [22]
E97-2	Air	ARBOR 1	30.2	330 [59]
		ARBOR 2	71.0	330 [22]
F82H	Vacuum	N/A	3.8	T_{irr}=250, T_{test}=RT [71]
				250 [71]
	Air	ARBOR 1	30.2	330 [59]

Table 2
Test conditions and sources for the database of LCF tests of nonirradiated RAFM steel specimens as obtained from open literature.

Material	Test medium	Test temperature (°C)											
		RT	150	250	300	330	350	400	450	500	550	600	650
E97-1	Air	[1]			[58]	[59]			[60,61]	[60,62]	[61]		[61]
	Vacuum		[1]	[63]	[1]		[63]		[63]		[1]		
E97-2	Air	[64]				[59]					[64–66]		
E97-3	Air	[67,68]			[68]		[67,68]		[68]		[68]		
F82H		[69,70]			[69]	[59]		[69]	[69]	[69]	[69]		
	Vacuum	[36,71]		[71]				[72]		[72]	[36]	[72]	[72]
JLF-1	Air	[73]											
	Vacuum	[73]						[73]				[73]	
ARAA	Air				[74]						[74]	[74]	
In-RAFM	Air	[75]						[75]	[75]		[75]	[75]	
CLAM	Air	[76]							[77]		[77,78]		

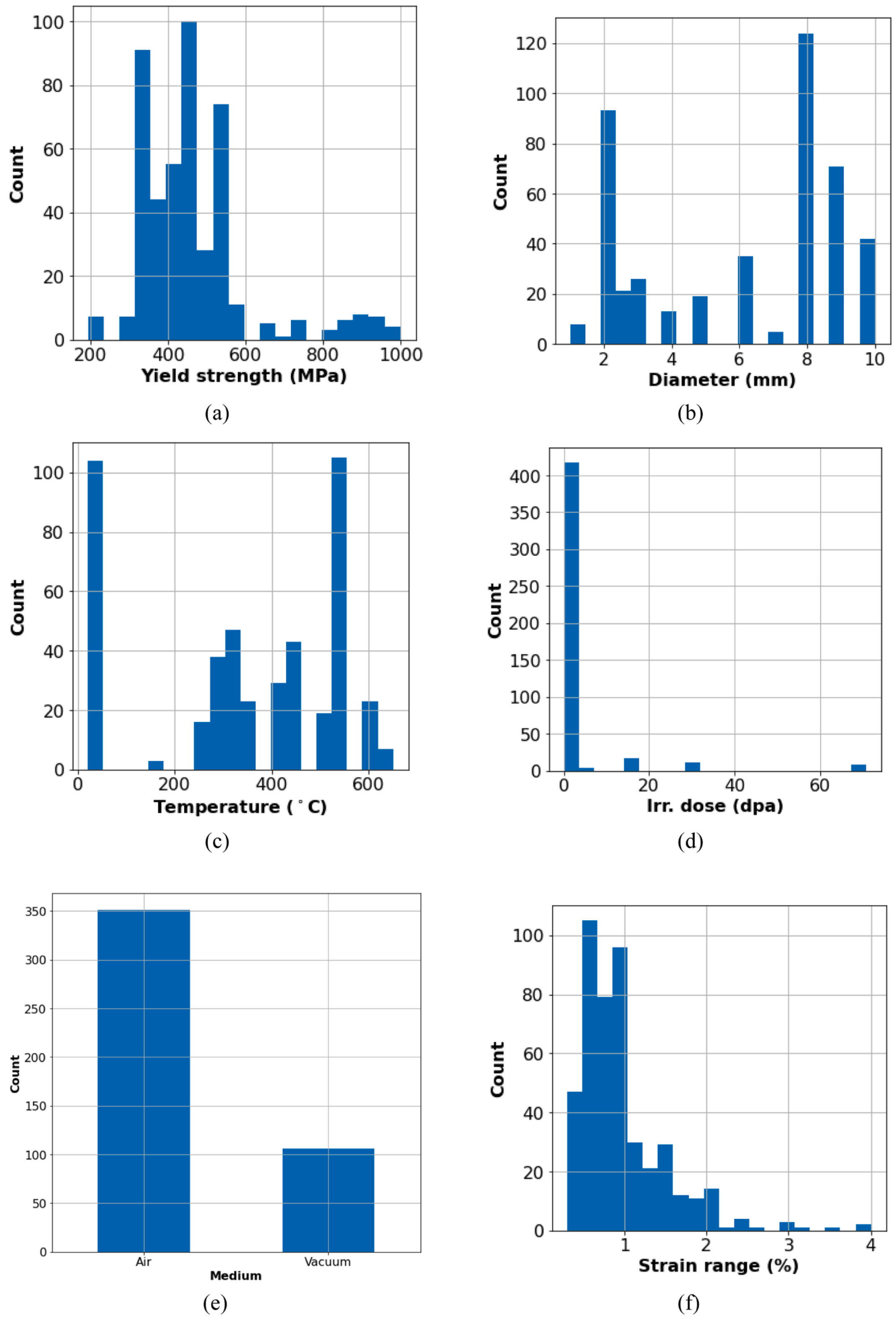

Fig. 1. Distribution of values of input parameters to the ML model: (a) Yield strength, (b) diameter, (c) temperature, (d) irradiation dose, (e) test medium, and (e) strain range.

prediction variance. In the context of this study, RF is particularly advantageous as it efficiently handles non-linear relationships and reduces sensitivity to outliers. These considerations are key given the heterogeneous test conditions and material variability in the LCF database.

A decision tree is divided into three parts: the root node for the input, the leaf node for the output, and the intermediate node. In the RF algorithm, a large number of decision trees is produced. The predictions of all decision trees are then averaged to give the final predicted value.

In the case of the LCF database, the RF algorithm receives an input feature vector composed of the LCF test conditions. By training on

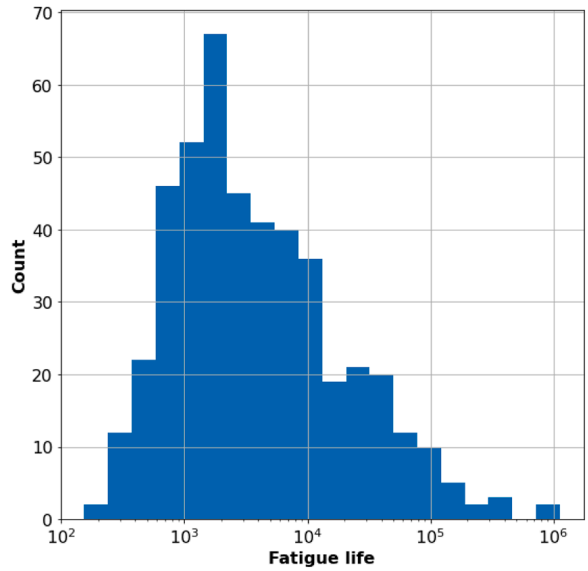

Fig. 2. Distribution of the output variable (fatigue life).

Table 4
Yield strengths of the analysed nonirradiated RAFM steels.

Material	Test temperature (°C)	Yield strength (MPa)	Material	Test temperature (°C)	Yield strength (MPa)
E97-1	23	532	F82H	23	540
[53]	150	503	[69]	250	476
	250	487		300	472
	300	473		330	469
	330	462		400	452
	350	454		450	434
	450	403		500	400
	500	370		550	353
	550	331		600	288
	650	194		650	201
E97-2	23	531	JLF-1	23	497
[88]	330	460	[89]	400	404
	550	317		600	316
E97-3	23	532	ARAA	300	445
[90,	300	465	[74]	550	356
91]	350	458		600	323
	450	440	In-	23	509
	550	339	RAFM	400	424
CLAM	23	576	[92]	450	413
[93]	450	404		550	373
	550	364		600	337

Table 5
Yield strengths of the analysed irradiated RAFM steels.

Material	Irradiation dose (dpa)	Irradiation/Test temperature (°C)	Yield strength (MPa)
E97-1	2.5	300 [58]	735
	16.3	250 [63]	877
		350 [63]	676
		450 [63]	415
	30.2	330 [59]	930
	71	330 [22]	947
E97-2	30.2	330 [59]	916
	71.0	330 [22]	998
F82H	3.8	RT [71]	823
		250 [71]	684
	30.2	330 [59]	913

various bootstrapped subsets of the data, each tree learns a slightly different mapping from the data to the predicted fatigue life. The averaging step for the predictions of all the different trees makes the RF algorithm more robust against outlier and noisy data in the LCF dataset. This is useful due to the variety of RAFM steels and test conditions included in this study. In particular, the ensemble nature of RF helps capture nonlinearities in how the different inputs interact to influence the fatigue life.

The main parameters to be defined for RF are the number of decision trees (200-2000), and the maximum depth of the tree (10-110) as shown later in Table 6.

SVR

SVR is a supervised ML algorithm designed to find the optimal regression line (or hyperplane) by maximizing the margin between predicted and actual values, using a kernel to model complex, non-linear relationships [97,98].Support vectors are the specific datapoints in the training set that lie closest to the regression hyperplane and directly determine its position and orientation. In SVR, only these points (rather than the entire dataset) influence the final model, making SVR both efficient and robust to capture intricate patterns within the fatigue life data by focusing on the most informative datapoints. This makes it well-suited for datasets with limited but diverse samples as in this study. The radial basis function (RBF) is chosen as the kernel model due to its high efficiency and accuracy, and the kernel parameter was chosen with a value of 0.1.

In the case of the LCF database, the kernel model captures the complex relationships between the input features vector and fatigue life. The parameter kernel parameter controls the kernel's reach, while the penalty parameter C manages the penalty for large errors. For instance, if certain datapoints deviate strongly from the rest, the SVR model can either allow for that deviation (when the value of C is small) or try to fit it more tightly (when the value of C) is large. The end result is a continuous function $f(x)$ that predicts the fatigue life for a given set of input parameters.

The main parameter to be defined for SVR is then the penalty parameter C (1-1000) as shown later in Table 6.

MLP

Artificial Neural Network (ANN) has widely been used to solve non-linear problems by acquiring knowledge through experience [99,100]. The key advantage of ANN is their flexibility to model subtle, high-dimensional interactions between test conditions allowing for accurate fatigue life predictions even when input-output relationships are not explicitly defined. A MLP-ANN [101] was used in this study.

Table 6
Hyperparameters determined for every algorithm for Scenario 1 and Scenario 2.

Algorithm	Hyperparameter	Grid range	Tuned value for scenario 1	Tuned value for scenario 2
RF	Number of decision trees	{200 – 2000}	1400	200
	Max depth of the tree	{10 – 110}	100	50
SVR	Penalty parameter	{1 – 1000}	100	10
MLP	Number of hidden layers	{1 – 5}	4	4
	Number of neurons in each hidden layer	{5 – 50}	45, 30, 20, 5	35, 30, 25, 5
GBR	Min samples to be a leaf node	{1 – 5}	3	4
	Min samples to split a leaf node	{1 – 50}	30	10
	Number of boosting iterations	{100 – 500}	200	200
	Subsample	{0.8 – 1.0}	0.9	0.9

A typical ANN consists of three types of layers: input, output, and one or more hidden layers, and each layer consists of a number of neurons. In this study, the rectified linear unit (ReLU) activation function was chosen passing the output of the neuron to the next layer. The learning rate was set at 0.001.

In the case of the LCF database, the input layer contains a number of neurons equal to the number of input features (five for scenario 1 and four for scenario 2). The output layer contains a single neuron whose activation represents the predicted fatigue life.

By stacking multiple hidden layers between the input and output layer, the MLP algorithm is capable of learning complex, highly non-linear relationships. This is beneficial where interactions between the different input features leads to significant variability in fatigue life. Once trained, the MLP algorithm an take any combination of these input features and yield a direct numerical prediction of fatigue life. The network's parameters (weights and biases) are iteratively update during the training process so that the difference between the predicted and actual fatigue life is minimized.

The main parameters to be defined for MLP are the number of hidden layers (1-5) and the number of neurons in each hidden layer (5-50) as shown later in Table 6.

GBR

GBR is an ensemble learning technique that builds a series of shallow decision trees (weak learners), each one correcting the errors of its predecessor in a stage-wise fashion [102]. Decision trees are used as prediction models here. The idea here is that the algorithm initializes the weak prediction model including the loss function to be minimized by the output parameter of the initial leaf nodes k. After each iteration, the pseudo-residuals are calculated as the negative gradient of the loss function of every sample where the learning rate (shrinkage parameter) in this study is set at 0.2.

In the case of the LCF database, each weak learner is a decision tree that uses the same input vector to give an estimate for the fatigue life. GBR starts with this simple estimate and iteratively refines it by fitting new trees to the residuals at each step. By adding weak learners in a stage-wise manner, the final model can capture subtle relationships such as how slight increments in the input features affect the overall fatigue performance. The learning rate controls how fast or slow the model corrects itself. Therefore, a moderate value (0.2 in this case) helps balance overfitting versus underfitting of the dataset.

The main parameters to be defined for GBR are the number of boosting iterations (100-500), the fraction of samples to be used for fitting (subsample of 0.8-1.0), the minimum number of samples required to split an internal node (1-50), and the minimum number of samples required to be a leaf node (1-5) as shown later in Table 6.

Feature selection

Mutual information assessment

An initial assessment was made on the whole dataset to quantify the importance of the different input vectors. Mutual information assessment was done to measure the dependency between the input vectors, and the target vector (fatigue life). This technique is based on the entropy estimation using k-nearest neighbours distances [103,104]. Mutual information assessment is calculated using the following equation [50]:

$$MI(Class,\ Attribute) = S(Class) - S(Class|Attribute) \tag{1}$$

where S(x) represents the information entropy. In mutual information, the higher the value, the higher the dependency. A value of zero represents no dependency. The input vectors included one tensile property that differentiates the different RAFM steels included in this study. The rest of the vectors were the fatigue test conditions.

Correlation matrix

The correlation analysis was performed on the input variables x, and the output variable (fatigue life) y in this study. The correlation coefficient is a value ranging from -1 to 1. A value of zero indicates no correlation at all, and a value of 1 or -1 indicates perfect positive or negative correlation respectively. It is calculated using the following equation:

$$PCC = \frac{\sum (x-\overline{x})(y-\overline{y})}{\sqrt{\sum (x-\overline{x})^2 \sum (y-\overline{y})^2}} \tag{2}$$

ML framework

The algorithms described in section 2.2 were implemented using scikit-learn library in python [105]. The database of LCF specimens was imported with the values of input features and targets as listed in section 2.1. The ML workflow then consisted of several steps: (i) Data loading and splitting, (ii) Data pre-processing (standardization), (iii) Hyperparameter tuning, (iv) Model training, (v) Model validation, and (vi) Final prediction. The ML workflow is summarized in the flow chart in Fig. 3. In the following subsections, each step is detailed in context of the LCF database.

Data loading and splitting

All data points (fatigue test results on RAFM steels) were gathered into a single database, where each row correspond to one fatigue test. The features (input variables) and the target (fatigue life) were separated out and labelled according.

The entire database was then randomly splits into three sets: training set (70 % of the datapoints) used for both training the model and performing the hyperparameter tuning, validation set (15 % of the datapoints) used after the model has been trained to check for overfitting and guide final hyperparameter adjustments, and prediction set (15 % of the datapoints) which is put aside and only used after the final hyperparameters have been chosen to provide an unbiased estimate of the model's performance on truly unseen data. This three-way split ensures that the final performance metrics are not overly optimistic due to repeated exposure of the data during hyperparameter tuning.

Data pre-processing

Before training, it is crucial to normalize or scale the input features and the target variable (fatigue life) so that large-values variables do not prevail over the smaller-valued ones during optimization. For this reason, their values were pre-processed using scikit-learn's StandardScaler function. This function normalizes each column in the dataset to have a mean of zero and a standard deviation of one [106]. Each input feature x is scaled according to the following equation:

$$x_{scaled} = \frac{x-\mu}{\sigma} \tag{3}$$

where μ and σ are the mean and standard deviation of that feature, computed only on the training set.

Specifically, the implementation of the pre-processing starts with computing the mean and standard deviation of each feature from the training set. Then the training set features are scaled accordingly. Finally, the same scaling is applied to both the validation and prediction sets. This procedure avoids any data leakage (i.e., ensures the information in the validation or prediction sets does not influence the model training or feature scaling).

Hyperparameter tuning

Each of the four algorithms (RF, SVR, MLP, and GBR) described in section 2.2 require a set of hyperparameters that strongly affects its performance (e.g., the number of estimators for RF, or the penalty parameter C for SVR). Therefore, the selection of these hyperparameters has to be done with care.

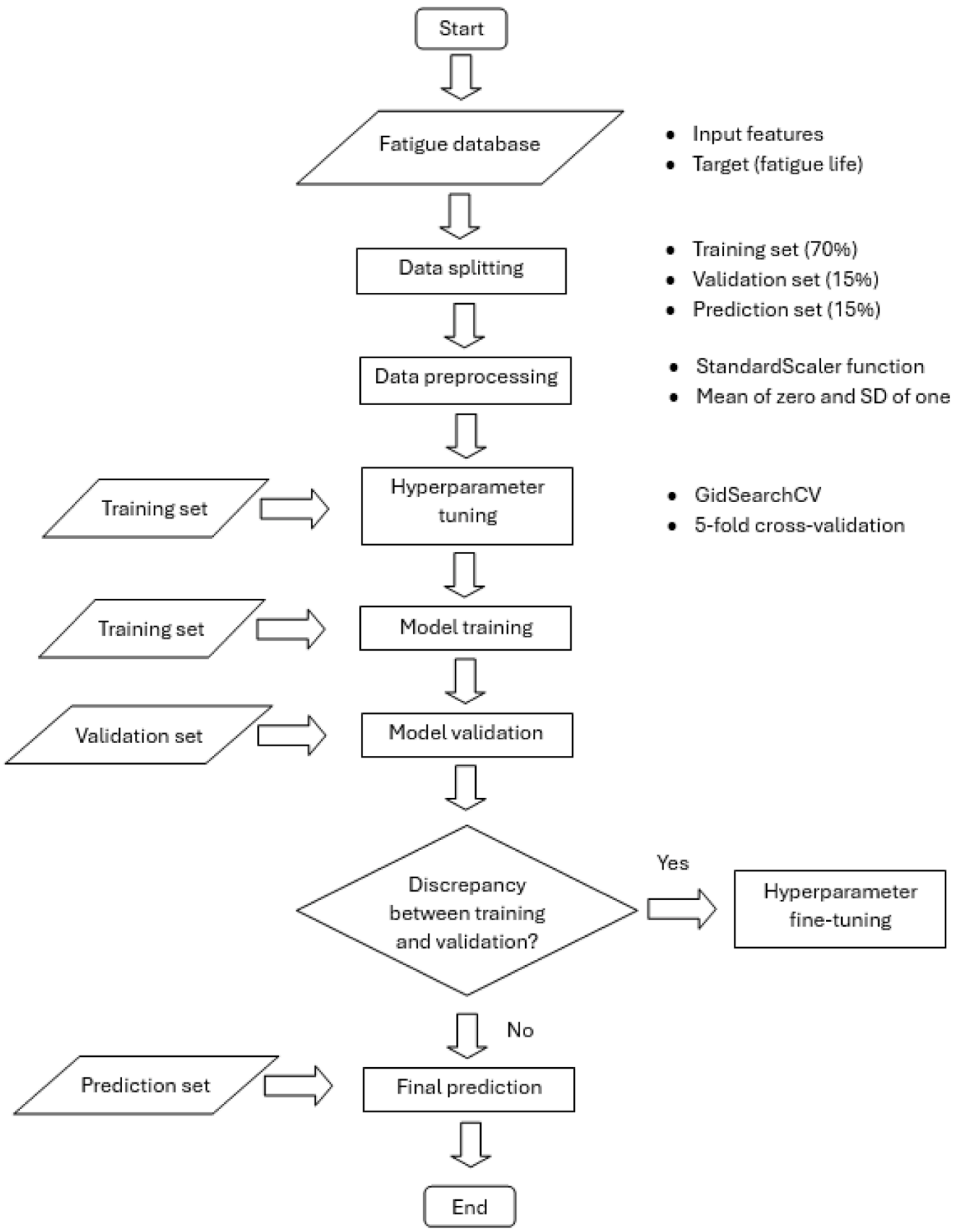

Fig. 3. Flowchart of the ML framework in this study.

In order to systematically search for the optimal hyperparameter values, Scikit-learn's GridSearchCV [107] was used in combination with a 5-fold cross-validation on the training set [108]. GridSearchCV was chosen as it exhaustively evaluates all combinations over the moderate-sized hyperparameter grids, which guarantees the reproducibility of results, and integrates seamlessly with scikit-learn's cross-validation pipeline. For each algorithm, a dictionary of possible hyperparameter values is created. For instance, in SVR, a dictionary of the penalty parameter C with values {1, 10, 100, 1000} is created. Similarly for all the hyperparameters of the rest of the algorithms. These values were chosen based on the typical values recommended in literature, expertise based on similar problems, and computational feasibility.

During the 5-fold cross-validation, the training set was further divided into five folds (subsets) of approximately equal size. In each iteration, four of the five folds were used to train the model with a specific hyperparameter combination, and the remaining fold was used for internal validation. This process is repeated five times, each using a different fold as the internal validation fold, ensuring all data in the training set was once used for internal validation.

For each hyperparameter combination, an average R^2 across the five folds was calculated. The average R^2 reflects how well each combination generalizes within the training set, mitigating the risk of overfitting a single subset. The best hyperparameters were then selected as those providing the highest average R^2 score over the five folds.

Model training and validation

Once the optimal hyperparameters were found via GridSearchCV, each algorithm was training using the training set. Scikit-learn's training routine has a built-in stopping criteria for each algorithm where training automatically stopped once the improvement per iteration slowed down below a preset threshold.

The trained algorithms were then evaluated on the validation set to assess whether their performance was significantly lower than on the training set. If a strong discrepancy was observed, the hyperparameters were finely tuned to avoid the problem of potential overfitting or underfitting. The final tuned hyperparameters and the ranges used for GridSearchCV for every algorithm are listed in Table 6.

Final prediction

After confirming an acceptable performance on both the training and validation sets, the trained algorithms with the chosen hyperparameters were fixed. These algorithms were then evaluated on the prediction set which has been completely put aside.

The scoring methods used to assess the final predictions of the four algorithms were R^2 and the mean absolute percentage error (MAPE) scores calculated using equations 20 and 21 respectively [109].

$$R^2 = 1 - \frac{\sum_{i=1}^{N}\left(y_i - y_i^{pred}\right)^2}{\sum_{i=1}^{N}\left(y_i - \bar{y}\right)^2} \tag{4}$$

$$MAPE = \frac{1}{N}\sum_{i=1}^{N}\frac{\left|y_i - y_i^{pred}\right|}{y_i} \times 100\ \% \tag{5}$$

These two metrics complement each other: R^2 highlights the variance explained by the model, while MAPE shows the relative prediction error, which is crucial in fatigue life predictions since they can span over several orders of magnitude.

Results and discussion

In this section, the results of running the ML algorithms on the fatigue database of irradiated and non-irradiated RAFM are shown in detail:

Feature selection

The mutual information assessment was performed separately on the irradiated and non-irradiated material datasets as shown in Fig. 4.

In Fig. 4a, it is shown that fatigue life has almost the same dependency on temperature, and yield strength for non-irradiated material. A similar observation was obtained from Fig. 4b where fatigue life has almost the same dependency on yield strength and irradiation dose for irradiated material. A reason for this could be the high correlation between yield strength and temperature, and yield strength and irradiation dose leading to these inputs providing the same information to the prediction of fatigue life. For non-irradiated material (Fig. 4a) it is shown that fatigue life has higher dependency on specimen diameter compared to the rest of the input vectors. Several studies confirmed that specimens with smaller diameters showed shorter fatigue lives [18,21,110]. This dependency was less evident for irradiated material (Fig. 4b) since LCF tests were always performed on irradiated specimens of diameters 4 mm or smaller. Medium is shown to have the smallest effect on fatigue life. It is important to mention that all the calculated dependencies were relatively low, as they all depend on the strain range as well. It is well known that strain range is the most influential parameter on fatigue as it directly contributes to the accumulated plastic strain. In order to fully capture the dependencies, LCF test performed at the same strain ranges under all test conditions should be available in the database which might not be the case in the gathered database.

An interesting observation is that the available dataset on irradiated material showed that fatigue life did not show any dependency on temperature or medium (values were below 10^{-3}) (Fig. 4b). The reason for this could be attributed to the relatively small database for irradiated RAFM steels gathered from literature. Several irradiation doses were included at a small temperature range (most of the tests were performed between 300 and 350°C) which enabled the assessment to capture the dependency the fatigue life on the irradiation dose. In addition to this, more tests would be required in a vacuum at the same test conditions of those performed in air to better capture the dependency of fatigue life on test medium. Still, as mentioned in the introduction, LCF tests performed on irradiated specimens are limited due to the technical and cost problems This further proves the need for alternative methods such as ML which are capable for capturing complex non-linear dependencies between the input features and fatigue life.

In order to analyse the similar dependency of fatigue life on yield strength and temperature for non-irradiated material, and yield strength and irradiation dose for irradiated material, a correlation analysis was

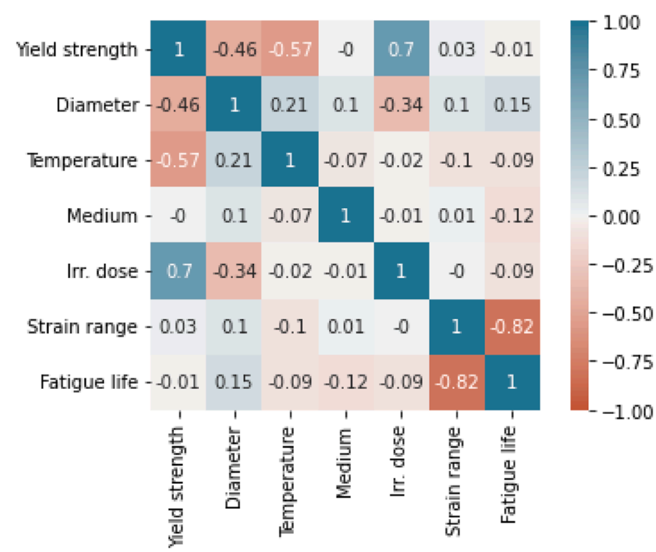

Fig. 5. Correlations between the input and output variables.

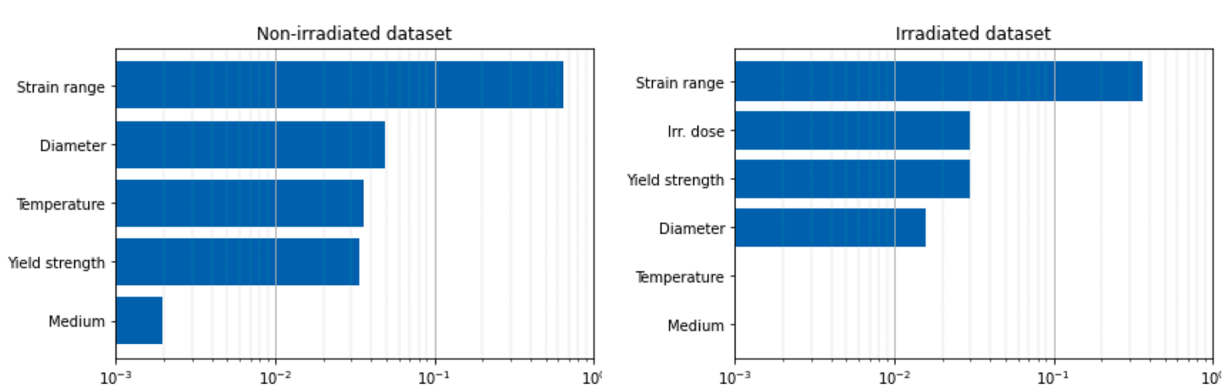

(a) (b)

Fig. 4. Mutual information assessment done on (a) non-irradiated dataset and (b) irradiated dataset.

made. The correlation matrix shown in Fig. 5 indicates low correlation between the different input variables. The exception is the yield strength which shows high correlation with temperature, and irradiation dose. It is well known that yield strength decreases with increased temperature. Yield strength was also reported to increase with irradiation. This increase is steep at low irradiation doses (<10 dpa) as the defect density increases with the irradiation dose. Then, the increase becomes less steep due to the annihilation of some of the newly formed defects by the already existing ones. The result is less newly formed defects until saturation is reached at high irradiation dose [22]. The aim of this study is to predict the fatigue life of RAFM steels at different irradiation doses. Thus, yield strength might not be the best representative at high doses and the direct use of the irradiation dose as input to the model in this case is preferred. This indicates that using yield strength along with the fatigue test conditions might be a source of redundancy in the inputs for the ML algorithms. The difference in yield strength was observed to be relatively small between the different RAFM steels at the same testing conditions.

An unexpected, high negative correlation was observed between yield strength and diameter. It can be attributed to the fact that LCF tests on irradiated material (with higher yield strength) were done on specimens with smaller diameters compared to non-irradiated material, introducing a bias. Another observation which confirms this statement is a large negative correlation between irradiation dose and diameter. Again, the correlation between the different input variables (except for strain range) and the output variable (fatigue life) are low. This is due to the fact that fatigue life highly depends on the applied strain range, so any effect of the rest of the input variables is combined with the effect of strain range.

Predictions using different algorithms

As described in section 2, the benchmarking of the different algorithms listed in section 2.2 were done using two scenarios (with and without yield strength as input). The performance of these algorithms assessed by R^2, and MAPE scores is shown in Fig. 6 and Fig. 7 respectively.

Typically, the accuracy scores are better on the training set compared to the validation set for all algorithms. As mentioned in section 3.4, the objective is to have the smallest difference between these accuracy scores as an indication for reduced overfitting. Hence, proving the ability of the algorithm to predict unseen test conditions.

Results show that RF gives the highest R^2 score on the training set (0.9696) closely followed by GBR (0.9552). However, the difference between the R^2 score on the training and validation sets is higher for RF compared to GBR (R^2 score on the validation set is 0.90577 for RF and 0.9247 for GBR) . This gives GBR an advantage over RF in the ability of the algorithm to predict unseen data. SVR shows the smallest difference between the R^2 score of the training and validation sets but overall lower scores than the two algorithms (0.9077 for training set and 0.9049 for validation set).

Another key observation is that the difference in the performance of the algorithms between Scenarios 1 and 2 is negligible. R^2 score for RF was 0.9623 and 0.9130, and for GBR was 0.9542 and 0.9249 on the training and validation sets respectively. This is in line with the fact that the difference in yield strength of the different RAFM steels at different temperatures and irradiation doses is small compared to the variance of the fatigue life of these steels even at identical testing conditions.

This was further observed in the MAPE scores on the training and validation sets where RF gave the lowest error score on the training set (0.3 % for Scenario 1 and 0.35 % for Scenario 2) while GBR gave the second lowest (0.4 % for Scenario 1 and 0.43 % for Scenario 2) but with significantly lower error score on the validation data (1 % and 1.2 % for RF compared to 0.7 and 0.75 % for GBR for Scenarios 1 and 2 respectively). Again, the difference between the MAPE scores for Scenarios 1 and 2 was very small.

The assessment of the prediction of RF and GBR algorithm was done by plotting the actual vs predicted fatigue lives using both scenarios (Fig. 8 using RF and Fig. 9 using GBR). In these Fig.s, the central diagonal solid line represents the one-to-one correspondence (meaning perfect prediction). The dashed lines were constructed as a sleeve limiting the spread by a factor of two from the central line. The predicted values of fatigue life represented by datapoints lying within this sleeve were considered accurate enough for the purpose of this study. In addition to this, points lying above the central line correspond to underprediction of fatigue life (conservative) and vice versa. The points were coloured to distinguish irradiated (red points) and non-irradiated (blue points) specimens.

It was observed that the datapoints lie around the central line indicating good fitting for the training set. Most of the points lay within the

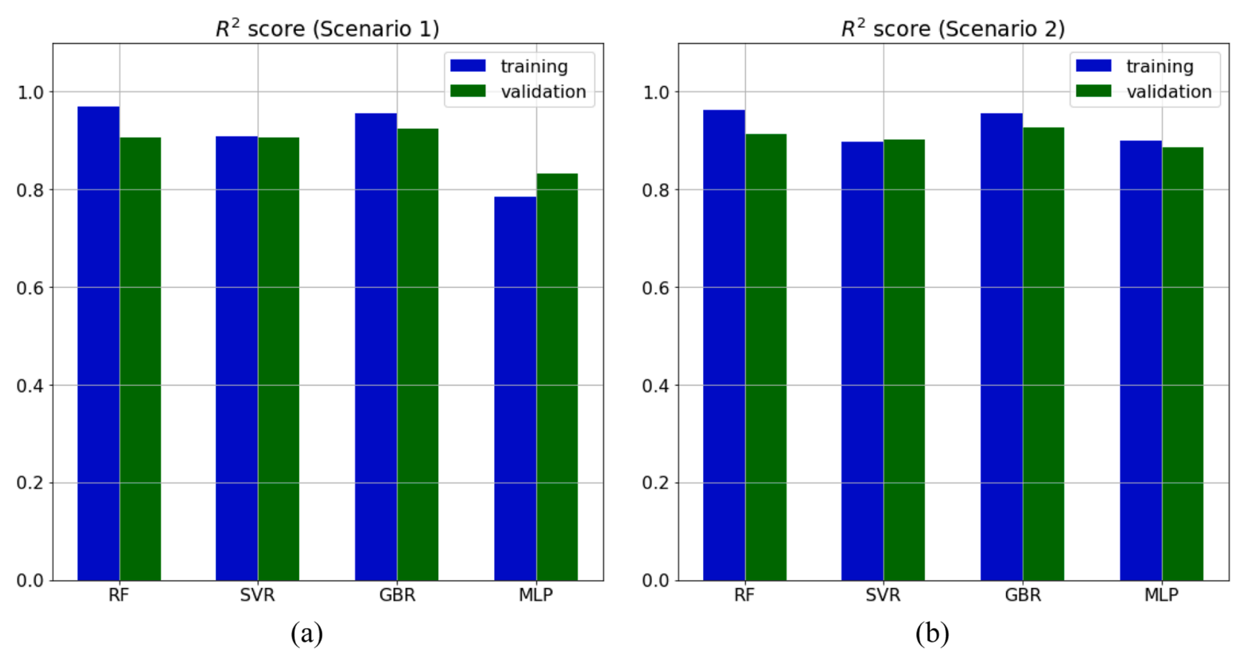

Fig. 6. R^2 score for the predictions of the ML algorithms on the training and validation sets on (a) Scenario 1 and (b) Scenario 2.

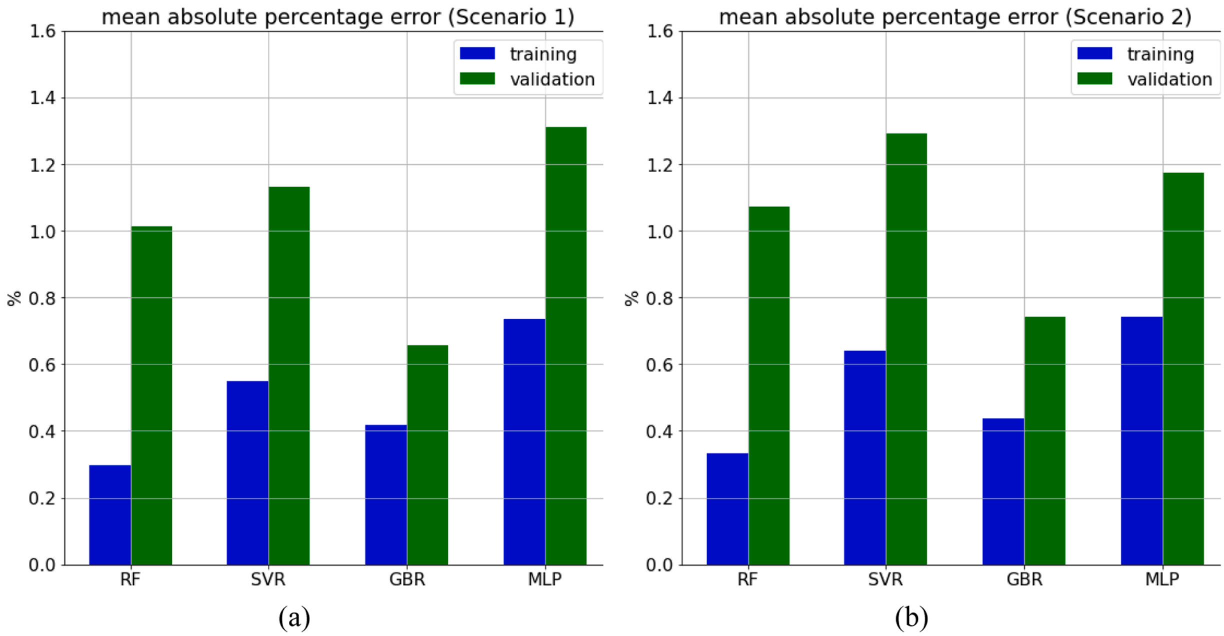

Fig. 7. MAPE score for the predictions of the ML algorithms on the training and validation sets on (a) Scenario 1 and (b) Scenario 2.

prediction sleeve within a factor of two for both the prediction and the validation sets. It was also observed that the variation in prediction was higher toward high number of cycles (higher than 50,000 cycles) corresponding to small strain ranges (smaller than 1 %). The distribution of fatigue life in Fig. 2 demonstrates that the database included less number LCF tests with very small or very high fatigue life. Still, the both models were able to predict the small fatigue life with higher accuracy. At these small strain ranges, the fatigue tests get closer to the high cycle fatigue regime with less plastic strain per cycle. Therefore, the fatigue life becomes more affected by the microstructural features (grain size, inclusions, dislocations, etc.) leading to larger variation in the experimental fatigue life.

In addition to this, the scatter of data for scenario 1 and scenario 2 was very similar for both algorithms. According to these observations, it can be concluded that GBR and RF are the best algorithms to predict the fatigue life of the irradiated and non-irradiated RAFM steels without the need to perform further tensile tests.

Shapley additive exPlanation (SHAP analysis)

The findings in the previous subsection revealed that RF and GBR algorithms showed the best training and validation scores. To further understand the performance differences between GBR and RF, SHAP analysis was conducted. The aim of the SHAP analysis is to assess how these algorithms handle the input data to make predictions. The SHAP analysis was performed separately on irradiated and non-irradiated datasets which allowed to identify distinct patterns in feature importance and model sensitivity. The summarized SHAP analysis for all input features (scenario 2) are shown in Fig. 10 and Fig. 11 for both RF and GBR on the non-irradiated and irradiated datasets respectively. These plots show a series of points for each input variable with each point represents a fatigue test from the gathered database. The x-axis represents SHAP value which represents the change in the mean of predictions due to the value of the input variable. A positive SHAP value means increasing the predicted fatigue life compared to the mean of predictions and vice-versa. The wider the spread, the more influential the input value is to the algorithm prediction.

Both algorithms identified the strain range as the most influential input variable whether for the irradiated or non-irradiated datasets. For the non-irradiated dataset, the SHAP summary plots showed that GBR assigned slightly higher importance to secondary features such as temperature and diameter, and captured clearer interaction gradients. The RF model, while consistent in ranking strain range as dominant, exhibited more compressed SHAP distributions, indicating a more conservative modelling of feature effects. This can be attributed to the sequential learning strategy of GBR, which enables it to iteratively refine predictions by focusing on difficult-to-predict samples. In contrast, RF averages over independently trained trees, which may dilute the influence of rare but important patterns in the data.

Further details on the way both algorithms process the interaction between the different input variables, SHAP dependence plots were generated. These plots are made for one input variable at a time but the points are coloured based on the values of another input variable which can reveal the interaction between these two variables. For instance, the plots in Fig. 12 show the interaction between the irradiation dose and strain using RF and GBR on the irradiated dataset. The x-axis in these figures represent the scaled value of the strain range and the y-axis represent the SHAP value of the strain range. The points are coloured based on the irradiation dose.

As expected, these plots show a decrease in the SHAP value with increasing strain range indicating the well-known observation that fatigue life becomes shorter at larger strain ranges. The coloured points reveal that the model tends to increase the predicted fatigue life for the same strain range after irradiation. This is similar to the observation by Gaganidze et al. [22]. The plots using RF and GBR show similar trends but still with a smaller range of SHAP values for RF compared to GBR. In addition to this, the colour pattern is stronger in GBR compared to RF.

These observations were made from the dependence plots of the different input variables whether on irradiated or non-irradiated datasets. From these observations, it can be concluded that GBR was more precisely able to capture the non-linear interactions between the features. The observed performance advantage of GBR over RF can be theoretically explained by their fundamental learning strategies. GBR is more sensitive to feature interactions and non-linearities, while RF tends to average out such interactions unless they are dominant across many trees. Furthermore, GBR's regularization mechanisms and adaptive focus on difficult samples make it more robust to the imbalanced nature of the dataset, particularly the limited number of irradiated specimens.

As indicated in section 4.1, the irradiation and test temperature range in the gathered database was relatively small. Therefore, the

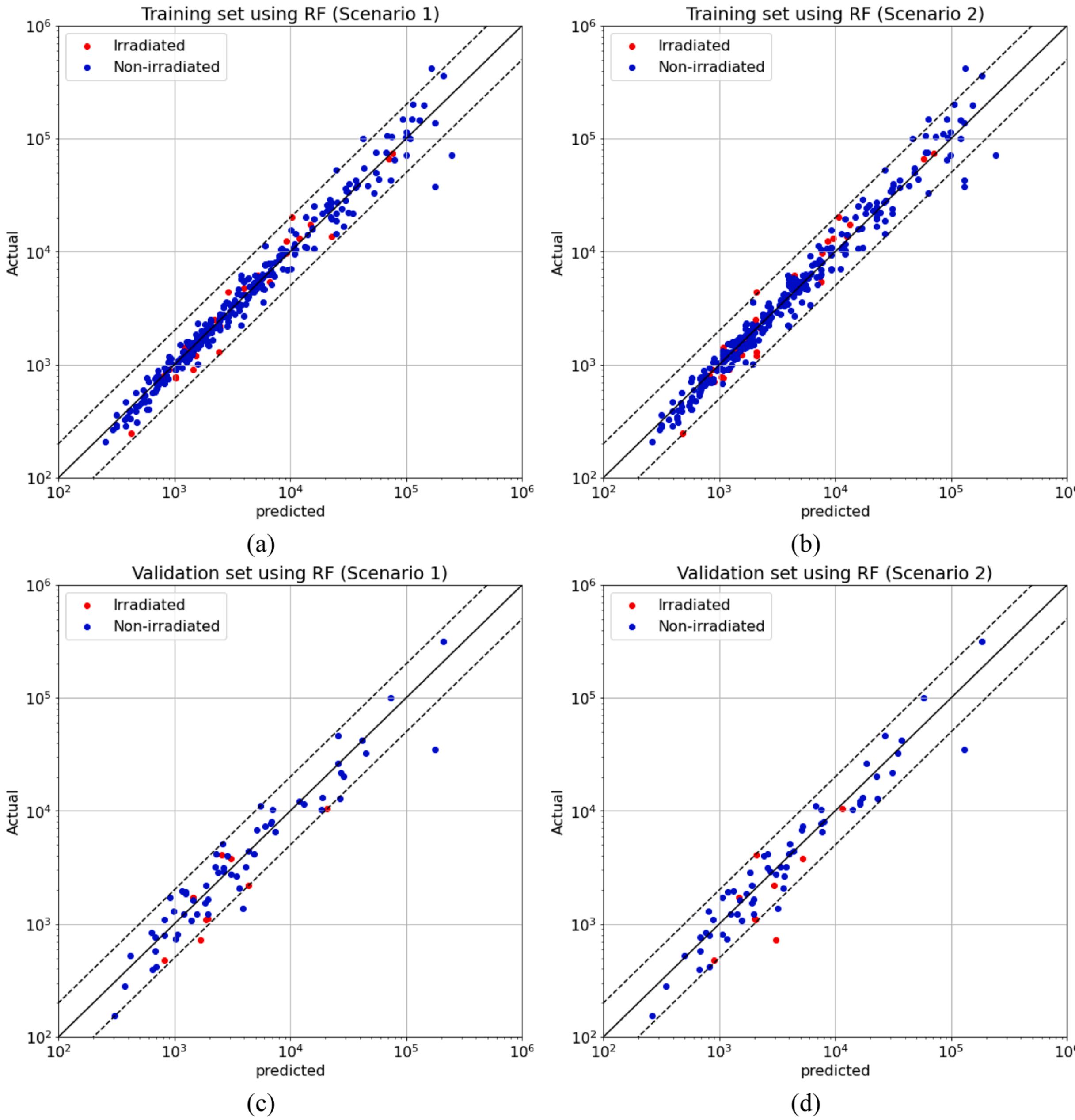

Fig. 8. Predicted vs actual fatigue life using RF on the training set using (a) Scenario 1 and (b) Scenario 2, and on the validation set using (c) Scenario 1 and (d) Scenario 2.

SHAP dependence plots were used to assess the sensitivity of the ML algorithms to the change in temperature. The plots are shown in Fig. 13 for temperature and its dependence on strain range for both RF and GBR on the irradiated dataset.

The dependence plots show that temperature still contributes to the fatigue life predictions. Moreover, the interaction with strain range (as indicated by colour gradients) suggests that the model captures complex dependencies even within this narrow band. The SHAP values of temperature on the irradiated dataset were slightly lower but still comparable to those obtained on the non-irradiated dataset and with a similar trend. This supports the robustness of the models' learned relationships despite the small temperature range. Again, GBR gave slightly larger SHAP value range compared to RF which further confirms the ability of GBR to capture the non-linear complex interactions between the input variables.

Assessment of the prediction of unseen data

As discussed in section 2.3, 15 % of the total dataset was put aside as a prediction set with a total of 69 datapoints. This means that this set was not used during the hyperparameter tuning of the algorithms. This set was used to assess the prediction capabilities of RF and GBR since they showed the best performance on the training and validation sets. The predicted vs actual fatigue life using RF and GBR are shown in Fig. 14 and Fig. 15 respectively using both scenarios. Again, the points were coloured to distinguish irradiated (red points) and non-irradiated (blue points) specimens.

The results in Fig. 14 and Fig. 15 show the capability of both algorithms with the chosen hyperparameters to predict the fatigue life of irradiated and non-irradiated RAFM steels. The datapoints seem to be distributed inside the sleeve with no systematic over or underprediction. Also, few datapoints lie outside the sleeve for both scenarios which was

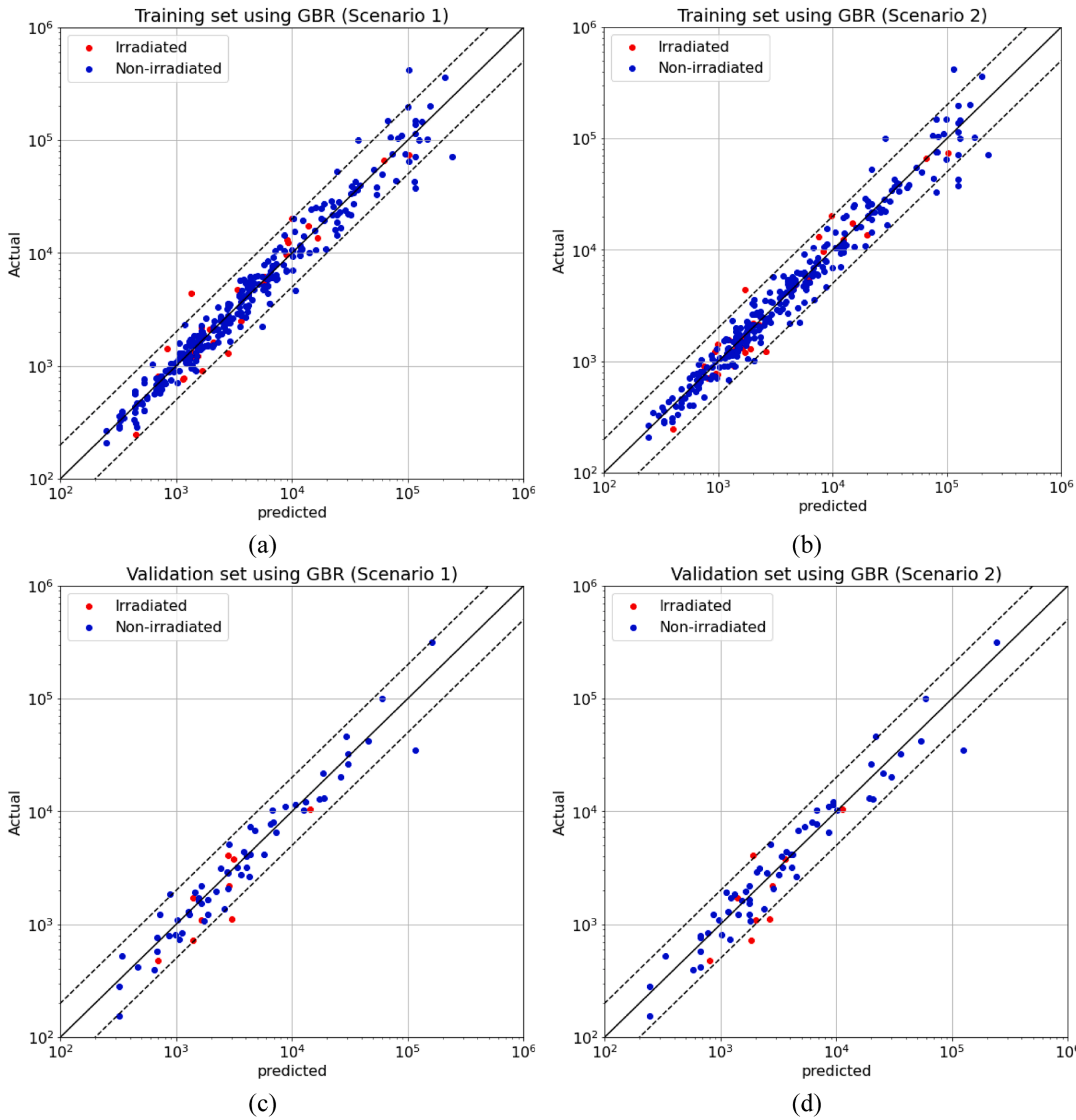

Fig. 9. Predicted vs actual fatigue life using GBR on the training set using (a) Scenario 1 and (b) Scenario 2, and on the validation set using (c) Scenario 1 and (d) Scenario 2.

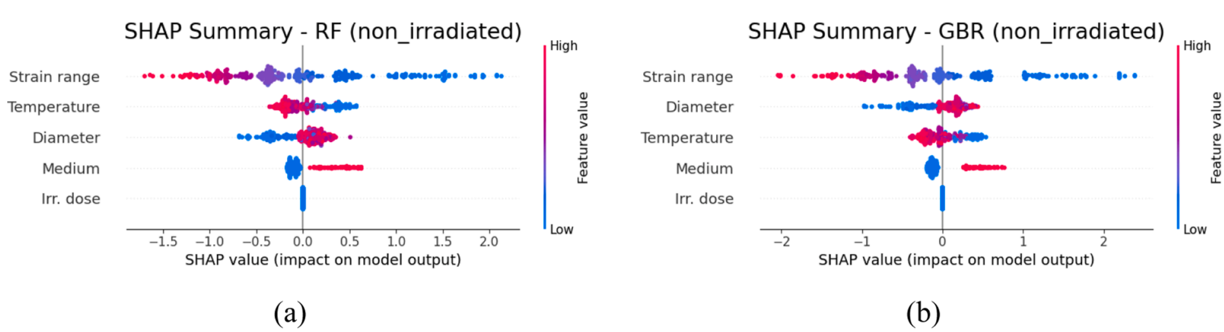

Fig. 10. SHAP summary for all input variable for the non-irradiated dataset using (a) RF, and (b) GBR.

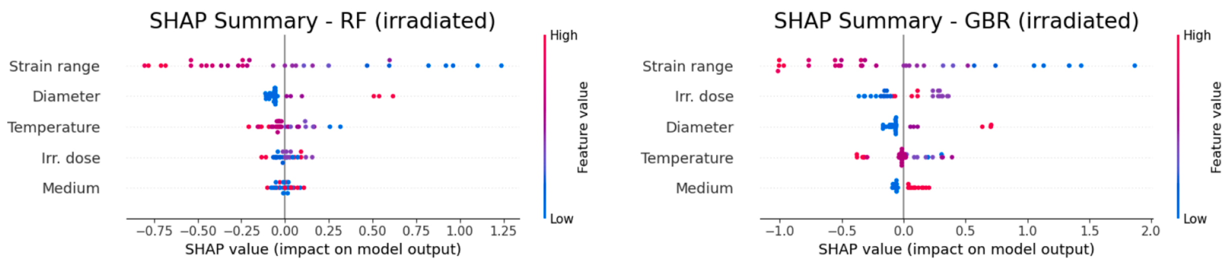

(a) (b)

Fig. 11. SHAP summary for all input variable for the irradiated dataset using (a) RF, and (b) GBR.

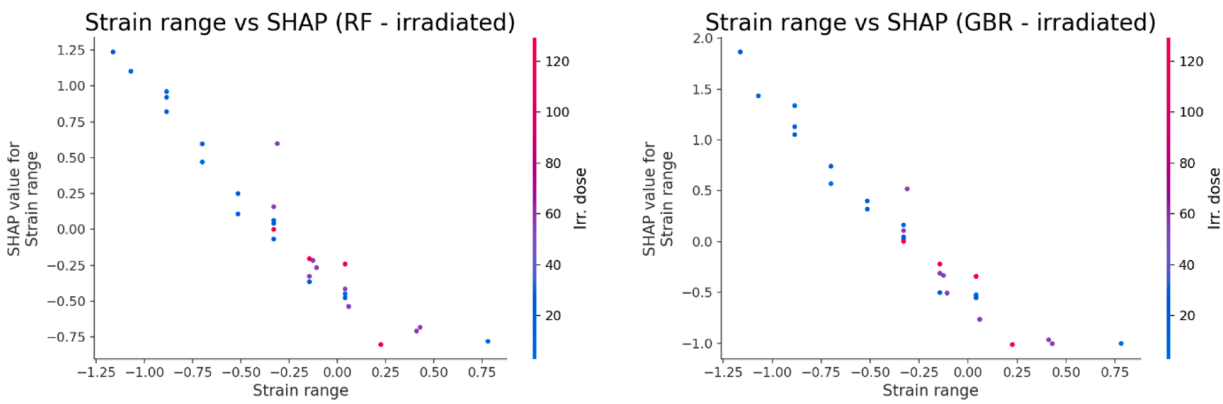

(a) (b)

Fig. 12. SHAP dependence plots between strain range and irradiation dose using (a) RF, and (b) GBR on the irradiated dataset.

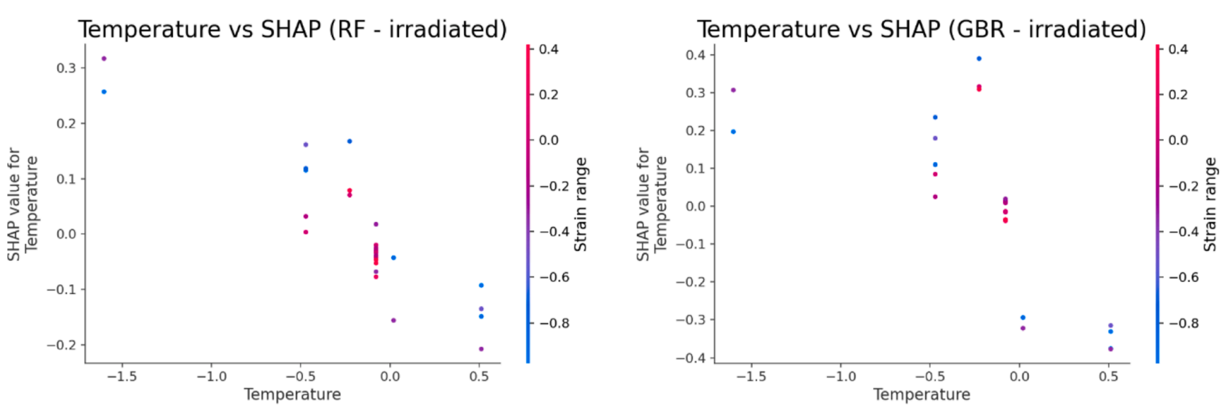

(a) (b)

Fig. 13. SHAP dependence plots between strain range and irradiation dose using (a) RF, and (b) GBR on the irradiated dataset.

considered a good prediction given the spread of the fatigue lives even for the same test conditions from the database included in this study.

The difference in prediction between Scenario 1 and Scenario 2 were negligible. This is a further observation confirming that the prediction of fatigue life could be done without the need for yield strength. This is beneficial when it comes to the prediction of fatigue life for RAFM steels at irradiation doses that have not yet been achieved.

The quality of the prediction of the GBR and RF algorithms for unseen test conditions using both scenarios is quantified in Table 7. The mean signed error and the standard deviation of the signed error were very close for both scenarios with a slight advantage for Scenario 2 using RF and Scenario 1 using GBR. The advantage of GBR over RF is the smaller scatter in the predicted fatigue life especially for the test conditions not included during the training process. The advantage of GBR over RF was also observed through the better R^2 and MAPE scores (0.9332 and 0.58 % for GBR compared to 0.9003 and 0.77 % for RF). This is an indication for the reduced overfitting of the training set by GBR leading to better accuracy when predicting the fatigue life under unseen test conditions. The values presented in the table demonstrate high accuracy of the proposed approach: 83-87 % of the predicted values of fatigue life (corresponding to unseen test conditions) lie within the factor of two sleeve. This is considered to be very good given the scatter of experimental fatigue life. Based on that, RF and GBR algorithms (with a slight advantage for the accuracy scores of GBR) are expected to give

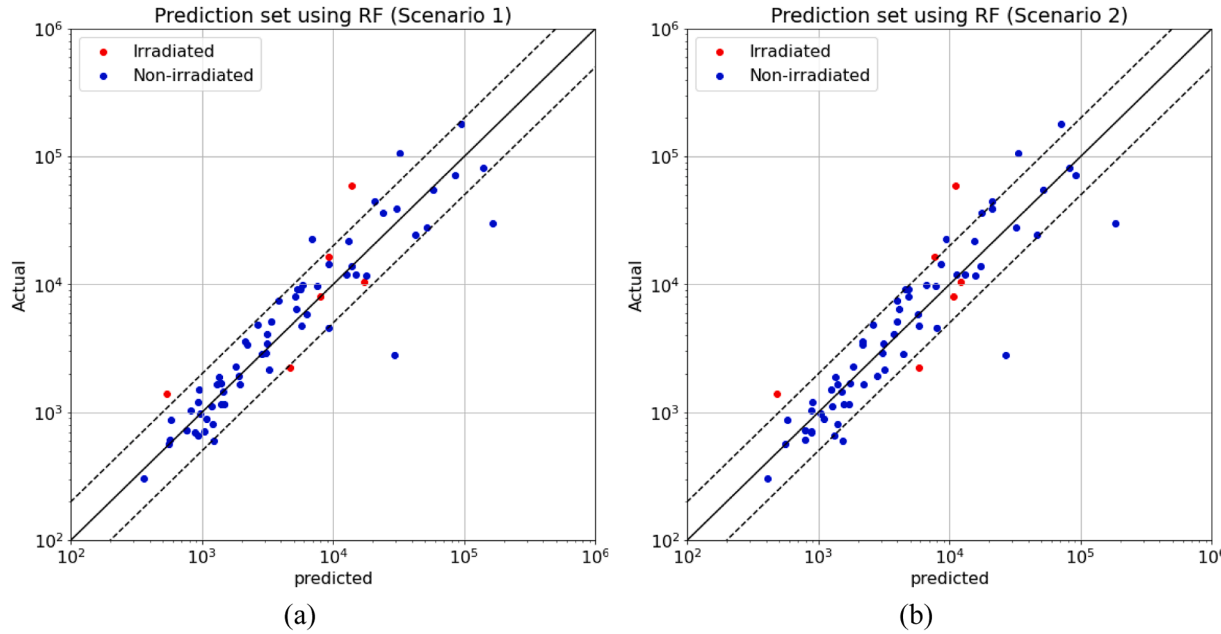

Fig. 14. Predicted vs actual fatigue life using RF on the prediction set (a) Scenario 1 and (b) Scenario 2.

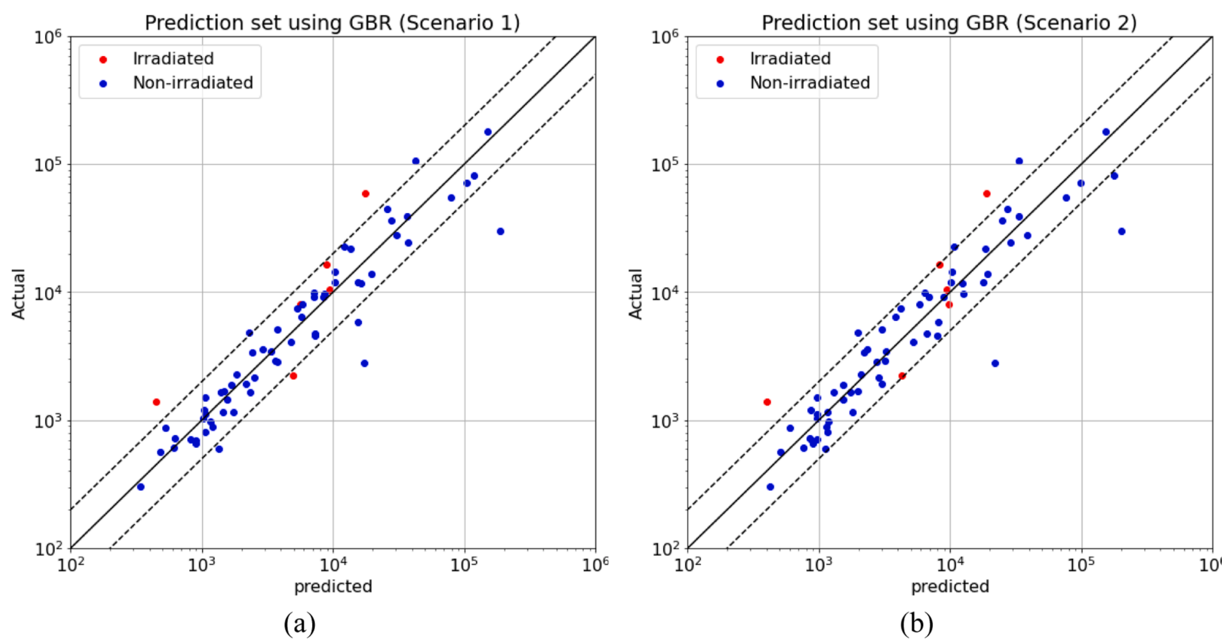

Fig. 15. Predicted vs actual fatigue life using RF on the prediction set (a) Scenario 1 and (b) Scenario 2.

Table 7
Quantification of the prediction accuracy of GBR algorithm for both scenarios.

Algorithm	Number of data points	Scenario	R^2	MAPE	Mean signed error	Standard deviation of signed error	Number of outlier points
RF	69	**Scenario 1**	0.9003	0.77 %	15.82 %	130.77 %	10
		Scenario 2	0.9005	0.69 %	15.50 %	125.13 %	12
GBR		**Scenario 1**	0.9332	0.58 %	18.78 %	92.29 %	9
		Scenario 2	0.9129	0.77 %	20.31 %	112.12 %	9

good prediction for unseen test conditions within the range of values of the attributes covered in this study. A separate study would be required for the extrapolation of the predictions on test conditions out of these ranges.

Conclusions

The aim of this work was to evaluate and provide new methods to characterise materials for structural components for fusion reactors without the need for performing numerous complicated LCF tests after neutron irradiation. Modern ML techniques were chosen to predict the fatigue life of RAFM steels under different test conditions could be made.

A total of 458 tests were gathered from literature with 408 tests on non-irradiated, and 50 on irradiated specimens. These tests cover a wide range of test temperatures (RT – 650°C), and irradiation doses (0-71 dpa). RF, SVR, MLP, and GBR algorithms were trained on 70 % of the database with 15 % used for the validation. The predictive power was finally assessed on the unseen 15 % of the dataset.

The findings demonstrate that using ML, it was possible to predict the fatigue life with high accuracy even without the need for tensile properties. Below, the main conclusions from this study are listed:

- GBR and RF algorithms gave the best prediction with high R^2 and MAPE scores. RF showed the highest scores on the training set (R^2 of 0.9696, and MAPE of 0.3 %), and GBR showed the highest scores on the validation set (R^2 of 0.9247, and MAPE of 0.7 %).
- The prediction of fatigue life for RAFM steels using Scenario 2 (without yield strength) was comparable to Scenario 1 (with yield strength). This was due to the high correlation between yield strength and test temperature for non-irradiated material, and yield strength and irradiation dose for irradiated material. The differences in yield strength of RAFM steels under the same test conditions were observed to be small.
- GBR and RF algorithms with the tuned parameters were able to predict the fatigue life of the irradiated and non-irradiated RAFM steels at unseen test conditions with 83-87 % of the points within a prediction sleeve within a factor of two.
- The advantage of GBR over RF is the smaller scatter in the predicted fatigue life, particularly for test conditions not included during training. This was attributed to the better ability of GBR to predict the complex non-linear interactions between the input variables.
- This study was limited by the LCF tests available in literature, especially for the irradiated specimens where most irradiated tests were conducted between 300-350°C. This limits the ability of the algorithms to generalize the predictions across broader temperature ranges. The more available tests, the better prediction capability of the ML algorithms.
- Future work can be done by integrating microstructural features before and after irradiation to improve model accuracy. Specifically, dislocation density, and the formation of dislocation loops and voids can be quantified using Transmission Electron Microscopy (TEM). Grain size distribution can also be characterized by Electron Backscatter Diffraction (EBSD). Incorporating these microstructural features into the ML models may enhance their predictive capability, particularly in capturing the effects of irradiation-induced microstructural evolution, such as vacancy and interstitial clustering, helium bubble formation, and swelling, on fatigue life.

CRediT authorship contribution statement

Hussein Zahran: Conceptualization, Investigation, Methodology, Software, Writing – original draft. **Aleksandr Zinovev:** Conceptualization, Data curation, Supervision, Writing – review & editing. **Dmitry Terentyev:** Funding acquisition, Project administration, Writing – review & editing. **Ali Aouf:** Software, Writing – review & editing. **Magd Abdel Wahab:** Writing – review & editing, Supervision, Investigation, Conceptualization.

Declaration of competing interest

The authors declare that they have no known competing financial interests or personal relationships that could have appeared to influence the work reported in this paper.

Acknowledgment

This work has been carried out within the framework of the EUROfusion Consortium, funded by the European Union via the Euratom Research and Training Programme (Grant Agreement No 101052200 — EUROfusion). Views and opinions expressed are however those of the author(s) only and do not necessarily reflect those of the European Union or the European Commission. Neither the European Union nor the European Commission can be held responsible for them. The work was also supported by FOD grant.

Data availability

Data will be made available on request.

References

[1] P. Marmy, T. Kruml, Low cycle fatigue of Eurofer 97, J. Nucl. Mater. 377 (1) (2008) 52–58, https://doi.org/10.1016/j.jnucmat.2008.02.054.
[2] L. Spolladore, R. Rossi, I. Wyss, P. Gaudio, A. Murari, M. Gelfusa, J. Contributors, Detection of MARFEs using visible cameras for disruption prevention, Fusion Eng. Des. 190 (2023), https://doi.org/10.1016/j.fusengdes.2023.113507.
[3] M. Lehnen, K. Aleynikova, P.B. Aleynikov, D.J. Campbell, P. Drewelow, N. W. Eidietis, Y. Gasparyan, R.S. Granetz, Y. Gribov, N. Hartmann, E.M. Hollmann, V.A. Izzo, S. Jachmich, S.H. Kim, M. Kocan, H.R. Koslowski, D. Kovalenko, U. Kruezi, A. Loarte, S. Maruyama, G.F. Matthews, P.B. Parks, G. Pautasso, R. A. Pitts, C. Reux, V. Riccardo, R. Roccella, J.A. Snipes, A.J. Thornton, P.C. de Vries, E.J. Contributors, Disruptions in ITER and strategies for their control and mitigation, J. Nucl. Mater. 463 (2015) 39–48, https://doi.org/10.1016/j.jnucmat.2014.10.075.
[4] R. Lindau, A. Möslang, M. Rieth, M. Klimiankou, E. Materna-Morris, A. Alamo, A. A.F. Tavassoli, C. Cayron, A.M. Lancha, P. Fernandez, N. Baluc, R. Schäublin, E. Diegele, G. Filacchioni, J.W. Rensman, B. van der Schaaf, E. Lucon, W. Dietz, Present development status of EUROFER and ODS-EUROFER for application in blanket concepts, Fusion Eng. Des. (2005) 989–996, https://doi.org/10.1016/j.fusengdes.2005.06.186, 75-79.
[5] Q.Y. Huang, F. Team, Development status of CLAM steel for fusion application, J. Nucl. Mater. 455 (1-3) (2014) 649–654, https://doi.org/10.1016/j.jnucmat.2014.08.055.
[6] C. Cabet, F. Dalle, E. Gaganidze, J. Henry, H. Tanigawa, Ferritic-martensitic steels for fission and fusion applications, J. Nucl. Mater. 523 (2019) 510–537, https://doi.org/10.1016/j.jnucmat.2019.05.058.
[7] Q. Huang, N. Baluc, Y. Dai, S. Jitsukawa, A. Kimura, J. Konys, R.J. Kurtz, R. Lindau, T. Muroga, G.R. Odette, B. Raj, R.E. Stoller, L. Tan, H. Tanigawa, A.A. F. Tavassoli, T. Yamamoto, F. Wan, Y. Wu, Recent progress of R&D activities on reduced activation ferritic/martensitic steels, J. Nucl. Mater. 442 (1-3) (2013) S2–S8, https://doi.org/10.1016/j.jnucmat.2012.12.039.
[8] S. Raju, B.Jeya Ganesh, A.K. Rai, R. Mythili, S. Saroja, E. Mohandas, M. Vijayalakshmi, K.B.S. Rao, B. Raj, Measurement of transformation temperatures and specific heat capacity of tungsten added reduced activation ferritic–martensitic steel, J. Nucl. Mater. 389 (3) (2009) 385–393, https://doi.org/10.1016/j.jnucmat.2009.02.030.
[9] Y.B. Chun, S.H. Kang, S. Noh, T.K. Kim, D.W. Lee, S. Cho, Y.H. Jeong, Effects of alloying elements and heat treatments on mechanical properties of Korean reduced-activation ferritic–martensitic steel, J. Nucl. Mater. 455 (1-3) (2014) 212–216, https://doi.org/10.1016/j.jnucmat.2014.05.063.
[10] R.L. Klueh, A.T. Nelson, Ferritic/martensitic steels for next-generation reactors, J. Nucl. Mater. 371 (1-3) (2007) 37–52, https://doi.org/10.1016/j.jnucmat.2007.05.005.
[11] E. Lucon, M. Decréton, E. van Walle, Mechanical characterization of EUROFER97 irradiated (0.32 dpa, 300°C), Fusion Eng. Des. 69 (1-4) (2003) 373–377, https://doi.org/10.1016/S0920-3796(03)00075-9.
[12] E. Gaganidze, H.C. Schneider, B. Dafferner, J. Aktaa, High-dose neutron irradiation embrittlement of RAFM steels, J. Nucl. Mater. 355 (1-3) (2006) 83–88, https://doi.org/10.1016/j.jnucmat.2006.04.014.
[13] E. Gaganidze, C. Petersen, E. Materna-Morris, C. Dethloff, O.J. Weiss, J. Aktaa, A. Povstyanko, A. Fedoseev, O. Makarov, V. Prokhorov, Mechanical properties and TEM examination of RAFM steels irradiated up to 70 dpa in BOR-60, J. Nucl. Mater. 417 (1-3) (2011) 93–98, https://doi.org/10.1016/j.jnucmat.2010.12.047.
[14] E. Gaganidze, J. Aktaa, Assessment of neutron irradiation effects on RAFM steels, Fusion Eng. Des. 88 (3) (2013) 118–128, https://doi.org/10.1016/j.fusengdes.2012.11.020.
[15] G. Pintsuk, G. Aiello, S.L. Dudarev, M. Gorley, J. Henry, M. Richou, M. Rieth, D. Terentyev, R. Vila, Materials for in-vessel components, Fusion Eng. Des. 174 (2022).DOI: 10.1016/j.fusengdes.2021.112994.
[16] M. Gorley, E. Diegele, S. Dudarev, G. Pintsuk, Materials engineering and design for fusion—Towards DEMO design criteria, Fusion Eng. Des. 136 (2018) 298–303, https://doi.org/10.1016/j.fusengdes.2018.02.012.
[17] H. Tanigawa, Technical challenges on material and design criteria development for fusion in-vessel components, Fusion Eng. Des. 133 (2018) 89–94, https://doi.org/10.1016/j.fusengdes.2018.05.047.

[18] H. Zahran, A. Zinovev, D. Terentyev, G. Aiello, M.Abdel Wahab, Prediction of low cycle fatigue life for neutron-irradiated and nonirradiated RAFM steels using their tensile properties, Int. J. Fatigue 190 (2025), https://doi.org/10.1016/j.ijfatigue.2024.108589.
[19] B. Fournier, S. Maxime, C. Christel, N. Michel, R. Véronique, B. Annick, P. André, High temperature creep–fatigue–oxidation interactions in 9–12%Cr martensitic steels, J. Nucl. Mater. (2009) 418–421, https://doi.org/10.1016/j.jnucmat.2008.12.139, 386-388.
[20] B. Fournier, M. Sauzay, C. Caes, M. Noblecourt, M. Mottot, A. Bougault, V. Rabeau, A. Pineau, Creep–fatigue–oxidation interactions in a 9Cr–1Mo martensitic steel. Part I: effect of tensile holding period on fatigue lifetime, Int. J. Fatigue 30 (4) (2008) 649–662, https://doi.org/10.1016/j.ijfatigue.2007.05.007.
[21] S. Nogami, C. Hisaka, M. Fujiwara, E. Wakai, A. Hasegawa, High temperature fatigue life evaluation using small specimen, Plasma Fusion Res. 12 (0) (2017) 1405022, https://doi.org/10.1585/pfr.12.1405022. –1405022.
[22] E. Gaganidze, C. Petersen, Post irradiation examination of RAF/M steels after fast reactor irradiation up to 71 dpa and < 340°C (ARBOR 2) : RAFM steels: metallurgical and mechanical characterisation., FZKA-7596, Institut für Materialforschung II, Programm Kernfusion, Association Forschungszentrum Kalrsruhe/EURATOM (2011), https://doi.org/10.5445/ksp/1000023594.
[23] S. Ye, B. Li, Q. Li, H.-P. Zhao, X.-Q. Feng, Deep neural network method for predicting the mechanical properties of composites, Appl. Phys. Lett. 115 (16) (2019), https://doi.org/10.1063/1.5124529.
[24] D.L. Naik, R. Kiran, Identification and characterization of fracture in metals using machine learning based texture recognition algorithms, Eng. Fract. Mech. 219 (2019), https://doi.org/10.1016/j.engfracmech.2019.106618.
[25] X. Ma, X. He, Z.C. Tu, Prediction of fatigue–crack growth with neural network-based increment learning scheme, Eng. Fract. Mech. (2021) 241, https://doi.org/10.1016/j.engfracmech.2020.107402.
[26] S. Romano, A. Brandão, J. Gumpinger, M. Gschweitl, S. Beretta, Qualification of AM parts: extreme value statistics applied to tomographic measurements, Mater. Des. 131 (2017) 32–48, https://doi.org/10.1016/j.matdes.2017.05.091.
[27] A. du Plessis, I. Yadroitsava, I. Yadroitsev, Effects of defects on mechanical properties in metal additive manufacturing: A review focusing on X-ray tomography insights, Mater. Des. 187 (2020), https://doi.org/10.1016/j.matdes.2019.108385.
[28] H. Bao, S. Wu, Z. Wu, G. Kang, X. Peng, P.J. Withers, A machine-learning fatigue life prediction approach of additively manufactured metals, Eng. Fract. Mech. 242 (2021), https://doi.org/10.1016/j.engfracmech.2020.107508.
[29] J. Aktaa, R. Schmitt, High temperature deformation and damage behavior of RAFM steels under low cycle fatigue loading: Experiments and modeling, Fusion Eng. Des. 81 (19) (2006) 2221–2231, https://doi.org/10.1016/j.fusengdes.2006.03.002.
[30] J. Aktaa, C. Petersen, Challenges in the constitutive modeling of the thermo-mechanical deformation and damage behavior of EUROFER 97, Eng. Fract. Mech. 76 (10) (2009) 1474–1484, https://doi.org/10.1016/j.engfracmech.2008.12.017.
[31] U. Führer, J. Aktaa, Modeling the cyclic softening and lifetime of ferritic-martensitic steels under creep-fatigue loading, Int. J. Mech. Sci. 136 (2018) 460–474, https://doi.org/10.1016/j.ijmecsci.2017.12.042.
[32] J. Aktaa, C. Petersen, Modeling the constitutive behavior of RAFM steels under irradiation conditions, J. Nucl. Mater. 417 (1-3) (2011) 1123–1126, https://doi.org/10.1016/j.jnucmat.2010.12.295.
[33] O. Basquin, The exponential law of endurance tests, Proc Am. Soc. Test Mater. (1910) 625–630.
[34] S.S. Manson, Behavior of materials under conditions of thermal stress, Natl. Advisory Committee for Aeronautics (1953).
[35] L.F. Coffin Jr., A study of the effects of cyclic thermal stresses on a ductile metal, Trans. Am. Soc. Mech. Eng. 76 (6) (2022) 931–949, https://doi.org/10.1115/1.4015020.
[36] T. Hirose, H. Sakasegawa, M. Nakajima, T. Kato, T. Miyazawa, H. Tanigawa, Effects of test environment on high temperature fatigue properties of reduced activation ferritic/martensitic steel, F82H, Fusion Eng. Des. 136 (2018) 1073–1076, https://doi.org/10.1016/j.fusengdes.2018.04.072.
[37] T. Hirose, T. Kato, H. Sakasegawa, H. Tanigawa, T. Nozawa, Evaluation of fatigue properties of reduced activation ferritic/martensitic steel, F82H for development of design criteria, Fusion Eng. Des. 160 (2020) 111823, https://doi.org/10.1016/j.fusengdes.2020.111823.
[38] S. Nogami, W. Guan, M. Toyota, A. Hasegawa, Fatigue life prediction of ferritic/martensitic steels based on universal slope equations and tensile properties obtained using small specimen, Fusion Eng. Des. 125 (2017) 330–336, https://doi.org/10.1016/j.fusengdes.2017.04.036.
[39] C. Petersen, A. Povstyanko, V. Prokhorov, A. Fedoseev, O. Makarov, M. Walter, Tensile and low cycle fatigue properties of different ferritic/martensitic steels after the fast reactor irradiation 'ARBOR 1, J. Nucl. Mater. (2009) 299–302, https://doi.org/10.1016/j.jnucmat.2008.12.112, 386-388.
[40] C. Wang, C. Shen, Q. Cui, C. Zhang, W. Xu, Tensile property prediction by feature engineering guided machine learning in reduced activation ferritic/martensitic steels, J. Nucl. Mater. 529 (2020), https://doi.org/10.1016/j.jnucmat.2019.151823.
[41] N.J. Sai, P. Rathore, K. Sridharan, A. Chauhan, Machine learning-based predictions of yield strength for neutron-irradiated ferritic/martensitic steels, Fusion Eng. Des. 195 (2023), https://doi.org/10.1016/j.fusengdes.2023.113964.
[42] X.C. Li, M.J. Zheng, X.Y. Yang, P.H. Chen, W.Y. Ding, A property-oriented design strategy of high-strength ductile RAFM steels based on machine learning, Mat. Sci. Eng. A-Struct. 840 (2022), https://doi.org/10.1016/j.msea.2022.142891.
[43] Y.C. Liu, H. Wu, T. Mayeshiba, B. Afflerbach, R. Jacobs, J. Perry, J. George, J. Cordell, J.Y. Xia, H. Yuan, A. Lorenson, H.T. Wu, M. Parker, F. Doshi, A. Politowicz, L.D. Xiao, D. Morgan, P. Wells, N. Almirall, T. Yamamoto, G. R. Odette, Machine learning predictions of irradiation embrittlement in reactor pressure vessel steels, NPJ. Comput. Mater. 8 (1) (2022), https://doi.org/10.1038/s41524-022-00760-4.
[44] C.C. Wang, C.G. Shen, X.J. Huo, C. Zhang, W. Xu, Design of comprehensive mechanical properties by machine learning and high-throughput optimization algorithm in RAFM steels, Nucl. Eng. Technol. 52 (5) (2020) 1008–1012, https://doi.org/10.1016/j.net.2019.10.014.
[45] Z. Zhan, H. Li, A novel approach based on the elastoplastic fatigue damage and machine learning models for life prediction of aerospace alloy parts fabricated by additive manufacturing, Int. J. Fatigue 145 (2021), https://doi.org/10.1016/j.ijfatigue.2020.106089.
[46] M. Zhang, C.-N. Sun, X. Zhang, P.C. Goh, J. Wei, D. Hardacre, H. Li, High cycle fatigue life prediction of laser additive manufactured stainless steel: A machine learning approach, Int. J. Fatigue 128 (2019), https://doi.org/10.1016/j.ijfatigue.2019.105194.
[47] L. He, Z. Wang, H. Akebono, A. Sugeta, Machine learning-based predictions of fatigue life and fatigue limit for steels, J. Mater. Sci. Technol. 90 (2021) 9–19, https://doi.org/10.1016/j.jmst.2021.02.021.
[48] N.J. Sai, P. Rathore, A. Chauhan, Machine learning-based predictions of fatigue life for multi-principal element alloys, Scr. Mater. 226 (2023), https://doi.org/10.1016/j.scriptamat.2022.115214.
[49] D. Dai, T. Xu, X. Wei, G. Ding, Y. Xu, J. Zhang, H. Zhang, Using machine learning and feature engineering to characterize limited material datasets of high-entropy alloys, Comput. Mater. Sci. 175 (2020), https://doi.org/10.1016/j.commatsci.2020.109618.
[50] A. Agrawal, P.D. Deshpande, A. Cecen, G.P. Basavarsu, A.N. Choudhary, S. R. Kalidindi, Exploration of data science techniques to predict fatigue strength of steel from composition and processing parameters, Integr. Mater. Manuf. Innov. 3 (1) (2014) 90–108, https://doi.org/10.1186/2193-9772-3-8.
[51] A. Agrawal, A. Choudhary, Deep materials informatics: Applications of deep learning in materials science, MRS. Commun. 9 (3) (2019) 779–792, https://doi.org/10.1557/mrc.2019.73.
[52] V.S. Srinivasan, A. Valsan, K.B.S. Rao, S.L. Mannan, B. Raj, Low cycle fatigue and creep-fatigue interaction behavior of 316L(N) stainless steel and life prediction by artificial neural network approach, Int. J. Fatigue 25 (12) (2003) 1327–1338, https://doi.org/10.1016/S0142-1123(03)00064-1.
[53] E. Gaganidze, F. Gillemot, I. Szenthe, M. Gorley, M. Rieth, E. Diegele, Development of EUROFER97 database and material property handbook, Fusion Eng. Des. 135 (2018) 9–14, https://doi.org/10.1016/j.fusengdes.2018.06.027.
[54] A. Kohyama, Y. Kohno, M. Kuroda, A. Kimura, F. Wan, Production of low activation steel; JLF-1, large heats - Current status and future plan, J. Nucl. Mater. 258 (1998) 1319–1323, https://doi.org/10.1016/S0022-3115(98)00198-6.
[55] S. Jitsukawa, M. Tamura, B. van der Schaaf, R.L. Klueh, A. Alamo, C. Petersen, M. Schirra, P. Spaetig, G.R. Odette, A.A. Tavassoli, K. Shiba, A. Kohyama, A. Kimura, Development of an extensive database of mechanical and physical properties for reduced-activation martensitic steel F82H, J. Nucl. Mater. 307 (2002) 179–186, https://doi.org/10.1016/S0022-3115(02)01075-9.
[56] Y.B. Chun, S.H. Kang, D.W. Lee, S. Cho, Y.H. Jeong, A. Zywczak, C.K. Rhee, Development of Zr-containing advanced reduced-activation alloy (ARAA) as structural material for fusion reactors, Fusion Eng. Des. 109 (2016) 629–633, https://doi.org/10.1016/j.fusengdes.2016.02.032.
[57] S.K. Albert, K. Laha, A.K. Bhaduri, T. Jayakumar, E. Rajendrakumar, Development of IN-RAFM steel and fabrication technologies for Indian TBM, Fusion Eng. Des. 109 (2016) 1422–1431.DOI: 10.1016/j.fusengdes.2015.12.005.
[58] N.V. Luzginova, J. Rensman, P. ten Pierick, J.B.J. Hegeman, Low cycle fatigue of irradiated and unirradiated Eurofer97 steel at 300°C, J. Nucl. Mater. 409 (2) (2011) 153–155, https://doi.org/10.1016/j.jnucmat.2010.09.017.
[59] C. Petersen, Post irradiation examination of RAF/M steels after fast reactor irradiation up to 33 dpa and < 340ºC (ARBOR 1), FZKA-7517, Institut für Materialforschung II, Programm Kernfusion,Association Forschungszentrum Kalrsruhe/EURATOM (2010), https://doi.org/10.5445/ir/270081166.
[60] N.V. Luzginova, J.W. Rensman, M. Jong, P. ten Pierick, T. Bakker, H. Nolles, Overview of 10 years of irradiation projects on Eurofer97 steel at High Flux Reactor in Petten, J. Nucl. Mater. 455 (1-3) (2014) 21–25, https://doi.org/10.1016/j.jnucmat.2014.03.028.
[61] J. Aktaa, M. Weick, M. Walter, High temperature creep-fatigue structural design criteria for fusion components built from EUROFER 97, FZKA-7309, Forschungszentrum Karlsruhe GmbH Technik und Umwelt (Germany). EURATOM, Inst. fuer Materialforschung, Programm Kernfusion (2007).
[62] P. Fernández, RAFM steel eurofer'97 as possible structural material for fusion device. Metallurgical characterization on as received condition and after simulated service conditions, Inorme técnico CIEMAT (2004).
[63] E. Materna-Morris, A. Möslang, H.C. Schneider, Tensile and low cycle fatigue properties of EUROFER97-steel after 16.3 dpa neutron irradiation at 523, 623 and 723 K, J. Nucl. Mater. 442 (1-3) (2013) S62–S66, https://doi.org/10.1016/j.jnucmat.2013.03.038.
[64] M. Roldán, E. Leon-Gutierrez, P. Fernández, A. Gómez-Herrero, Deformation behaviour and microstructural evolution of EUROFER97-2 under low cycle fatigue conditions, Mater. Charact. 158 (2019) 109943, https://doi.org/10.1016/j.matchar.2019.109943.
[65] J. Aktaa, M. Walter, E. Gaisina, M.H.H. Kolb, R. Knitter, Assessment of the chemical compatibility between EUROFER and ceramic breeder with respect to

fatigue lifetime, Fusion Eng. Des. 157 (2020) 111732, https://doi.org/10.1016/j.fusengdes.2020.111732.
[66] K. Zhang, M. Walter, J. Aktaa, Ratcheting and fatigue behavior of Eurofer97 at high temperature, part 1: experiment, Fusion Eng. Des. 150 (2020) 111407, https://doi.org/10.1016/j.fusengdes.2019.111407.
[67] H. Zahran, A. Zinovev, D. Terentyev, X. Wang, M.Abdel Wahab, Experimental investigation and constitutive material modelling of low cycle fatigue of EUROFER97 for fusion applications, J. Nucl. Mater. 588 (2024) 154809, https://doi.org/10.1016/j.jnucmat.2023.154809.
[68] A. Zinovev, P. Lamagnere, K. Poleshchuk, D. Terentyev, D. Bernardi, C. Cristalli, E. Leon-Gutierrez, N. García-Rodríguez, C. Caes, G. Pintsuk, G. Aiello, Low cycle fatigue of EUROFER97 investigated for test blanket modules of ITER: an interlaboratory study, J. Nucl. Mater. 597 (2024), https://doi.org/10.1016/j.jnucmat.2024.155127.
[69] T. Nozawa, H. Tanigawa, T. Kojima, T. Itoh, N. Hiyoshi, M. Ohata, T. Kato, M. Ando, M. Nakajima, T. Hirose, J.D. Reed, X. Chen, J.W. Geringer, Y. Katoh, The status of the Japanese material properties handbook and the challenge to facilitate structural design criteria for DEMO in-vessel components, Nucl. Fusion 61 (11) (2021) 116054, https://doi.org/10.1088/1741-4326/ac269f.
[70] S. Nogami, Y. Sato, A. Tanaka, A. Hasegawa, A. Nishimura, H. Tanigawa, Effect of Specimen Shape on the Low Cycle Fatigue Life of Reduced Activation Ferritic/Martensitic Steel, J. Nucl. Sci. Technol. 47 (1) (2010) 47–52, https://doi.org/10.3327/jnst.47.47.
[71] Y. Miwa, S. Jitsukawa, M. Yonekawa, Fatigue properties of F82H irradiated at 523 K to 3.8 dpa, J. Nucl. Mater. 329 (2004) 1098–1102, https://doi.org/10.1016/j.jnucmat.2004.04.029.
[72] T. Ishii, K. Fukaya, Y. Nishiyama, M. Suzuki, M. Eto, Low cycle fatigue properties of 8Cr-2WVTa ferritic steel at elevated temperatures, J. Nucl. Mater. 258 (1998) 1183–1186, https://doi.org/10.1016/S0022-3115(98)00183-4.
[73] H.L. Li, A. Nishimura, T. Nagasaka, T. Muroga, Stress-strain behavior on tensile and low cycle fatigue tests of JLF-1 steel at elevated temperature in vacuum, Fusion Eng. Des. 81 (23-24) (2006) 2907–2912, https://doi.org/10.1016/j.fusengdes.2006.07.055.
[74] G.K. Ahiale, W.D. Choi, S.Y. Cho, Y.H. Park, Y.B. Chun, Y.J. Oh, Low-Cycle Fatigue Behavior of Reduced Activation Ferritic-Martensitic Steel at Elevated Temperatures (vol 29, pg 71, 2023), Met. Mater. Int. 29 (7) (2023) 2118, https://doi.org/10.1007/s12540-023-01410-0. –2118.
[75] K. Mariappan, V. Shankar, R. Sandhya, K. Laha, Low cycle fatigue design data for India-specific reduced activation ferritic-martensitic (IN-RAFM) steel, Fusion Eng. Des. 104 (2016) 76–83, https://doi.org/10.1016/j.fusengdes.2016.02.021.
[76] X. Hu, L.X. Huang, W.G. Wang, Z.G. Yang, W. Sha, W. Wang, W. Yan, Y.Y. Shan, Low cycle fatigue properties of CLAM steel at room temperature, Fusion Eng. Des. 88 (11) (2013) 3050–3059, https://doi.org/10.1016/j.fusengdes.2013.08.001.
[77] X. Hu, L.X. Huang, W. Yan, W. Wang, W. Sha, Y.Y. Shan, K. Yang, Low cycle fatigue properties of CLAM steel at 823 K, Mat. Sci. Eng. A-Struct. 613 (2014) 404–413, https://doi.org/10.1016/j.msea.2014.06.069.
[78] Y.Y. Zhao, X.W. Zhai, S.J. Liu, Low cycle fatigue properties of CLAM steel at 450°C and 550°C, Fusion Eng. Des. 112 (2016) 213–217, https://doi.org/10.1016/j.fusengdes.2016.08.015.
[79] Z. Zhan, H. Li, Machine learning based fatigue life prediction with effects of additive manufacturing process parameters for printed SS 316L, Int. J. Fatigue 142 (2021), https://doi.org/10.1016/j.ijfatigue.2020.105941.
[80] Z. Lian, M. Li, W. Lu, Fatigue life prediction of aluminum alloy via knowledge-based machine learning, Int. J. Fatigue 157 (2022), https://doi.org/10.1016/j.ijfatigue.2021.106716.
[81] W.Q. Hao, L. Tan, X.G. Yang, D.Q. Shi, M.L. Wang, G.L. Miao, Y.S. Fan, A physics-informed machine learning approach for notch fatigue evaluation of alloys used in aerospace, Int. J. Fatigue 170 (2023), https://doi.org/10.1016/j.ijfatigue.2023.107536.
[82] J. Yang, G. Kang, Y. Liu, Q. Kan, A novel method of multiaxial fatigue life prediction based on deep learning, Int. J. Fatigue 151 (2021), https://doi.org/10.1016/j.ijfatigue.2021.106356.
[83] X. Li, M. Zheng, X. Yang, P. Chen, W. Ding, A property-oriented design strategy of high-strength ductile RAFM steels based on machine learning, Mater. Sci. Eng. A 840 (2022), https://doi.org/10.1016/j.msea.2022.142891.
[84] K.C. Sahoo, J. Vanaja, P. Parameswaran, V.D. Vijayanand, K. Laha, Effect of thermal ageing on microstructure, tensile and impact properties of reduced activated ferritic-martensitic steel, Mater. Sci. Eng. A 686 (2017) 54–64, https://doi.org/10.1016/j.msea.2017.01.030.
[85] C. Mao, C. Liu, L. Yu, H. Li, Y. Liu, The correlation among microstructural parameter and dynamic strain aging (DSA) in influencing the mechanical properties of a reduced activated ferritic-martensitic (RAFM) steel, Mater. Sci. Eng. A 739 (2019) 90–98, https://doi.org/10.1016/j.msea.2018.10.023.
[86] Q. Wang, W. Wang, J. Wang, P. Du, H. Xu, Z. Yu, Y. Xu, H. Zhou, G. Luo, Effect of the cooling behavior on phase transformation and mechanical property of RAFM steel, J. Nucl. Mater. 600 (2024), https://doi.org/10.1016/j.jnucmat.2024.155272.
[87] O. Kachko, A. Puype, D. Terentyev, G. Bonny, W.V. Renterghem, R.H. Petrov, Development of RAFM steels for high temperature applications guided by thermodynamic modelling, Nucl. Mater. Energy 32 (2022), https://doi.org/10.1016/j.nme.2022.101211.
[88] E. Lucon, W. Vandermeulen, Overview and Critical Assessment of the Tensile Properties of unirradiated and irradiated EUROFER97, BLG–1042, Belgian Nucl. Res. Center SCK-CEN (Belgium) (2007).
[89] H. Li, A. Nishimura, T. Muroga, T. Nagasaka, Microstructural analysis on JLF-1 steel tested by fatigue deformation, J. Nucl. Mater. (2007) 147–152, https://doi.org/10.1016/j.jnucmat.2007.03.152, 367-370.
[90] A. Zinovev, C.-C. Chang, J. Van Eyken, E. Gaganidze, D. Terentyev, Effect of neutron irradiation to 0.7 and 1.4 dpa on the tensile mechanical properties and microstructure of EUROFER97 steel, Sci. Talks 6 (2023) 100214, https://doi.org/10.1016/j.sctalk.2023.100214.
[91] A. Zinovev, C.-C. Chang, J. Van Eyken, E. Gaganidze, D. Terentyev, Effect of neutron irradiation to 0.7 dpa and 1.4 dpa on the tensile properties and fracture surface of EUROFER97 steel, J. Nucl. Mater. 587 (2023), https://doi.org/10.1016/j.jnucmat.2023.154742.
[92] J. Vanaja, K. Laha, M. Nandagopal, S. Sam, M.D. Mathew, T. Jayakumar, E. R. Kumar, Effect of tungsten on tensile properties and flow behaviour of RAFM steel, J. Nucl. Mater. 433 (1-3) (2013) 412–418, https://doi.org/10.1016/j.jnucmat.2012.10.040.
[93] Y.F. Li, T. Nagasaka, T. Muroga, Q.Y. Huang, Y.C. Wu, Effect of thermal ageing on tensile and creep properties of JLF-1 and CLAM steels, J. Nucl. Mater. (2009) 495–498, https://doi.org/10.1016/j.jnucmat.2008.12.149, 386-388.
[94] S.Chehreh Chelgani, S.S. Matin, J.C. Hower, Explaining relationships between coke quality index and coal properties by Random Forest method, Fuel 182 (2016) 754–760, https://doi.org/10.1016/j.fuel.2016.06.034.
[95] M. Belgiu, L. Drăguţ, Random forest in remote sensing: A review of applications and future directions, ISPRS J. Photogramm. Remote Sens. 114 (2016) 24–31, https://doi.org/10.1016/j.isprsjprs.2016.01.011.
[96] V. Yarasu, B. Podgornik, An optimized machine-learning tool to predict heat treatment response of hot-work tool steels, Results Eng. 26 (2025), https://doi.org/10.1016/j.rineng.2025.105260.
[97] V.D.Sánchez A, Advanced support vector machines and kernel methods, Neurocomputing 55 (1-2) (2003) 5–20, https://doi.org/10.1016/s0925-2312(03)00373-4.
[98] W.S. Noble, What is a support vector machine? Nat. Biotechnol. 24 (12) (2006) 1565–1567, https://doi.org/10.1038/nbt1206-1565.
[99] N. Artrith, A. Urban, An implementation of artificial neural-network potentials for atomistic materials simulations: Performance for TiO2, Comput. Mater. Sci. 114 (2016) 135–150, https://doi.org/10.1016/j.commatsci.2015.11.047.
[100] B. Lotfi, P. Beiss, Application of neural networking for fatigue limit prediction of powder metallurgy steel parts, Mater. Des. 50 (2013) 440–445, https://doi.org/10.1016/j.matdes.2013.03.002.
[101] J. Paredes, D. Chávez, R. Isa-Jara, D. Vargas, A hybrid machine learning algorithm approach to predictive maintenance tasks: A comparison with machine learning algorithms, Results Eng. 26 (2025), https://doi.org/10.1016/j.rineng.2025.105137.
[102] J.H. Friedman, Stochastic gradient boosting, Comput. Stat. Data An. 38 (4) (2002) 367–378. DO I: Pii S0167-9473(01)00065-2.
[103] A. Kraskov, H. Stogbauer, P. Grassberger, Estimating mutual information, Phys. Rev. E Stat. Nonlin. Soft. Matter. Phys. 69 (6 Pt 2) (2004) 066138, https://doi.org/10.1103/PhysRevE.69.066138.
[104] B.C. Ross, Mutual information between discrete and continuous data sets, PLoS. One 9 (2) (2014) e87357, https://doi.org/10.1371/journal.pone.0087357.
[105] F. Pedregosa, G. Varoquaux, A. Gramfort, V. Michel, B. Thirion, O. Grisel, M. Blondel, P. Prettenhofer, R. Weiss, V. Dubourg, J. Vanderplas, A. Passos, D. Cournapeau, M. Brucher, M. Perrot, E. Duchesnay, Scikit-learn: machine learning in python, J. Mach. Learn. Res. 12 (2011) 2825–2830.
[106] N. Zamri, M.A. Pairan, W.N.A.W. Azman, S.S. Abas, L. Abdullah, S. Naim, Z. Tarmudi, M. Gao, A comparison of unsupervised and supervised machine learning algorithms to predict water pollutions, Procedia Comput. Sci. 204 (2022) 172–179, https://doi.org/10.1016/j.procs.2022.08.021.
[107] Pirjatullah, D. Kartini, D.T. Nugrahadi, Muliadi, A. Farmadi, Hyperparameter tuning using GridsearchCV on the comparison of the activation function of The ELM method to the classification of pneumonia in toddlers, 2021 4th International Conference on Computer and Informatics Engineering (Ic2ie 2021) (2021) 390–395.DOI: 10.1109/Ic2ie53219.2021.9649207.
[108] Y. Jung, Multiple predicting K-fold cross-validation for model selection, J. Nonparametr. Stat. 30 (1) (2017) 197–215, https://doi.org/10.1080/10485252.2017.1404598.
[109] C. Yazici, F.J. Domínguez-Gutiérrez, Machine learning techniques for estimating high–temperature mechanical behavior of high strength steels, Results Eng. 25 (2025), https://doi.org/10.1016/j.rineng.2025.104242.
[110] E. Gaisina, R. Gaisin, J. Leys, R. Knitter, J. Aktaa, M. Walter, Comparative analysis of low cycle fatigue behavior of pre-corroded standard and sub-sized EUROFER97 specimens exposed to ceramic breeder environment, Nucl. Mater. Energy 36 (2023) 101497, https://doi.org/10.1016/j.nme.2023.101497.